DNA Sequence and Ancillary Ligand Modulate the Biexponential Emission Decay of Intercalated [Ru(L) 2 dppz] 2+ Enantiomers

ARTICLE *in* CHEMISTRY - A EUROPEAN JOURNAL · NOVEMBER 2012

Impact Factor: 5.73 · DOI: 10.1002/chem.201201279 · Source: PubMed

4 AUTHORS, INCLUDING:

Johanna Andersson
Chalmers University of Technology
13 PUBLICATIONS **211** CITATIONS
SEE PROFILE

Eimer M Tuite
Newcastle University
43 PUBLICATIONS **1,915** CITATIONS
SEE PROFILE

CHEMISTRY
A EUROPEAN JOURNAL

ChemPubSoc
Europe

DOI: 10.1002/chem.201201279

DNA Sequence and Ancillary Ligand Modulate the Biexponential Emission Decay of Intercalated $[Ru(L)_2dppz]^{2+}$ Enantiomers

Andrew W. McKinley,[b] Johanna Andersson,[c] Per Lincoln,[c] and Eimer M. Tuite*[a]

Abstract: The bi-exponential emission decay of $[Ru(L)_2dppz]^{2+}$ (L = *N*,*N*′-diimine ligand) bound to DNA has been studied as a function of polynucleotide sequence, enantiomer, and nature of L (phenanthroline vs. bipyridine). The lifetimes (τ_i) and pre-exponential factors (α_i) depend on all three parameters. With $[poly(dA\text{-}dT)]_2$, the variation of α_i with [Nu]/[Ru] has little dependence on L for Λ-$[Ru(L)_2dppz]^{2+}$ but a substantial dependence for Δ-$[Ru(L)_2dppz]^{2+}$. With $[poly(dG\text{-}dC)]_2$, by contrast, the Λ-enantiomer α_i values depend strongly on the nature of L, whereas those of the Δ-enantiomer are relatively unaffected. DNA-bound linked dimers show similar photophysical behaviour. The lifetimes are identified with two geometries of minor-groove intercalated $[Ru(L)_2dppz]^{2+}$, resulting in differential water access to the phenazine nitrogen atoms. Interplay of cooperative and anti-cooperative binding resulting from complex–complex and complex–DNA interactions is responsible for the observed variations of α_i with binding ratio. $[Ru(phen)_2dppz]^{2+}$ emission is quenched by guanosine in DMF, which may further rationalise the shorter lifetimes observed with guanine-rich DNA.

Keywords: DNA · intercalation · luminescence lifetimes · photochemistry · ruthenium

Introduction

Ruthenium polypyridyl complexes are amongst the most studied inorganic compounds of the past 30 years, particularly with respect to their photophysical behaviour.[1] In general, they are chemically and photochemically stable and inert to substitution and racemisation. Moreover, their luminescence characteristics, redox properties, and excited-state reactivities can be tuned by variation of the polypyridyl ligands. They continue to be important components of functional supramolecular assemblies, and are included as light-harvesting antennae and photoinduced charge-separation modules in artificial photosynthesis systems. Cationic complexes of this class bind well to DNA, and have been used as luminescent probes, electron transfer relays, and therapeutic agents.[2–4]

$[Ru(bpy)_2dppz]^{2+}$ and $[Ru(phen)_2dppz]^{2+}$ (bpy = bipyridine; phen = phenanthroline; dppz = dipyrido[3,2-*a*:2′,3′-*c*]phenazine; Figure 1) and related complexes have aroused intense interest for two reasons that lend them to many applications: their ability to intercalate between the DNA base pairs and the extraordinary polarity dependence of their dppz-based ^{3}MLCT luminescence.[5] These "light-switch" complexes are effectively non-emissive in water,[6] but have their luminescence turned on when water is excluded, such as in organic solvents,[7,8] when incorporated in SDS micelles[9] and lipid environments,[10] and when intercalated with DNA.[11,12] This effect has been proposed to originate from two close-lying excited states with different rates

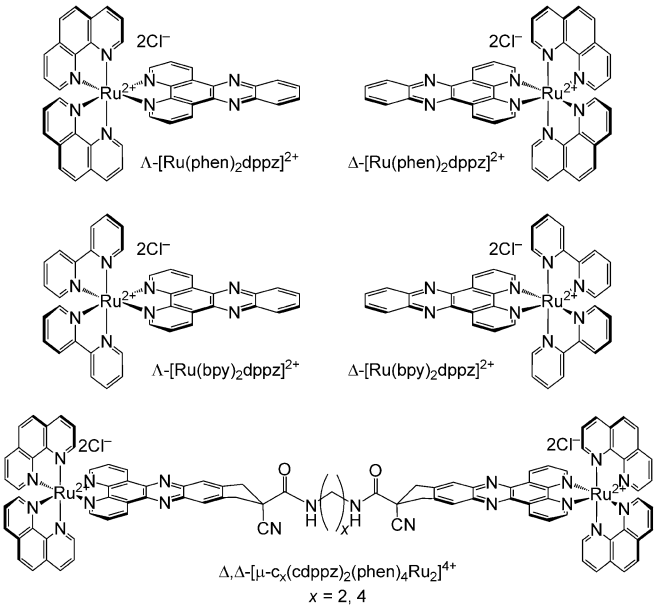

Figure 1. Structures of the studied complexes.

[a] Dr. E. M. Tuite
School of Chemistry, Bedson Building
Newcastle University, Newcastle upon Tyne, NE7 7RZ (UK)
Fax: (+44) 191-222-6929
E-mail: e.m.tuite@ncl.ac.uk

[b] Dr. A. W. McKinley
Department of Chemistry
Imperial College London, London SW7 2AZ (UK)

[c] Dr. J. Andersson, Dr. P. Lincoln
Department of Chemical and Biological Engineering
Chalmers University of Technology, 41296 Gothenburg (Sweden)

Supporting information for this article is available on the WWW under http://dx.doi.org/10.1002/chem.201201279.

of non-radiative decay, which are differentially populated in different environments.[5] Enhanced population of the non-emissive state is promoted by polar solvents and those with H-bonding ability.[13,14] Therefore, the dark state is dominant in water where it is related to formation of H -bonds between the water molecules and the 5,10-nitrogen atoms on the extended (phenazine) part of the dppz ring system,[15,16] with a requirement for both phenazine nitrogen atoms to be H -bonded to completely extinguish luminescence.[16]

The luminescence properties of $[Ru(L)_2dppz]^{2+}$ (L = polypyridyl ligand) when bound to DNA depend on a number of factors including DNA sequence, complex enantiomer, and the nature of the ancillary ligands.[17–19] When bound to DNA, the emission decay is almost invariably bi-exponential. We have previously reported preliminary observations regarding the variation in lifetimes of Δ- and Λ-$[Ru(phen)_2dppz]^{2+}$ bound to different sequences and conformations of nucleic acids.[18] For a single enantiomer with $[poly(dA\text{-}dT)]_2$, two discrete lifetimes are observed and their relative amplitudes vary with the Ru/nucleotide ([Nu]/[Ru]) ratio. Under the conditions studied, we never observed a monoexponential decay for $[Ru(L)_2dppz]^{2+}$ bound to DNA, which suggests a degree of binding cooperativity in all cases. Longer lifetimes are generally observed for the Δ-enantiomer and in AT-rich sequences. For the enantiomers with mixed sequences, for example, calf-thymus DNA, both the magnitude of the lifetimes and their relative amplitudes vary with [Nu]/[Ru].[12] Grow-in of the emissive state of DNA-bound $[Ru(phen)_2dppz]^{2+}$ on picosecond timescales is also bi-exponential,[19–21] suggesting that the two emission lifetimes arise from two DNA binding modes, rather than from excited-state interactions.

Different models have been proposed, or could be envisaged, to explain the observation of two lifetimes when $[Ru(phen)_2dppz]^{2+}$ binds to nucleic acids. These include two orientations of the complex when it binds from the major groove,[22] isolated and contiguously bound complexes in the minor groove,[12] or complexes bound alternately in the major and minor grooves. Recently, a new model has been developed[23] that reflects some elements of these ideas. It invokes cooperative and anti-cooperative interactions between complexes bound in symmetric and canted conformations and provides an excellent multivariate fit of photophysical and calorimetry data for $[Ru(bpy)_2dppz]^{2+}$ and $[Ru(phen)_2dppz]^{2+}$ bound to $[poly(dA\text{-}dT)]_2$. To investigate how this model relates to binding with other polynucleotides, we report here our examination of the luminescence lifetimes of ruthenium–dppz complexes under a wide variety of conditions in order to construct a general model. Recently published crystal structures of $[Ru(TAP)_2dppz]^{2+}$ and $[Ru(phen)_2dppz]^{2+}$ with oligonucleotides[24,25] place the metal complexes in the minor groove; this is consistent with previous NMR studies of related dppz complexes.[26,27] Our previous work reported preliminary lifetime results for $[Ru(phen)_2dppz]^{2+}$ enantiomers bound to different nucleic acids at a fixed [Nu]/[Ru] of 10.[18] In the current work, we report on the variation of lifetimes with binding ratio and ancillary ligand, in addition to sequence and enantiomer.

Results

$[Ru(phen)_2dppz]^{2+}$ emission with alternating homo-polynucleotides: As previously reported,[12,18] both enantiomers of $[Ru(phen)_2dppz]^{2+}$ exhibit two lifetimes when intercalated with the alternating DNA homopolymer $[poly(dA\text{-}dT)]_2$ (Tables S1 and S2 in the Supporting Information). Figure 2 illustrates the variation with [Nu]/[Ru] of the relative pre-exponential factors (α_i) for the long (τ_L) and short (τ_S) lifetime components for Δ- and Λ-$[Ru(phen)_2dppz]^{2+}$ bound to $[poly(dA\text{-}dT)]_2$.

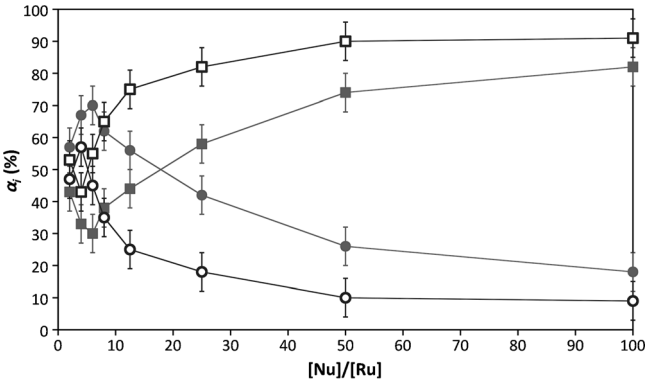

Figure 2. Pre-exponential factors (α_i) for enantiomers of $[Ru(phen)_2dppz]^{2+}$ bound to $[poly(dA\text{-}dT)]_2$ in phosphate buffer (5 mM, pH 6.9); Δ-enantiomer: closed symbols, $\tau_L = 732(\pm 38)$ ns (●), $\tau_S = 134(\pm 10)$ ns (■); Λ-enantiomer: open symbols, $\tau_L = 327(\pm 15)$ ns (○), $\tau_S = 42(\pm 6)$ ns (□); [Ru] = 20 μM; $\lambda_{ex} = 440$ nm; $\lambda_{em} > 540$ nm.

This graphical presentation of data facilitates comparison of pre-exponential factors in different systems. For both enantiomers with $[poly(dA\text{-}dT)]_2$, the relative contributions of each lifetime to the emission intensity (the amplitudes, f_i), and the related pre-exponential factors (α_i) vary with binding ratio such that τ_S dominates, but is not exclusive, at [Nu]/[Ru] = 100 (i.e., 25 base pairs per complex). With increasing amounts of $[Ru(phen)_2dppz]^{2+}$ bound to $[poly(dA\text{-}dT)]_2$, the proportion of the long-lived excited state increases. The lifetimes remain approximately constant during the titration until [Nu]/[Ru] < 4, at which point both lifetimes decrease, probably due to self-quenching by externally bound dye when all intercalation sites are filled. These trends led Hiort et al.[12] to assign the short lifetime to emission from isolated bound molecules and the long lifetime to that from contiguously bound molecules, whilst acknowledging the inconsistency of this model with the similar amplitudes observed at low binding ratios. With $[poly(dA\text{-}dT)]_2$, the lifetimes for Δ-$[Ru(phen)_2dppz]^{2+}$ are threefold larger than those for Λ-$[Ru(phen)_2dppz]^{2+}$, indicating that intercalated dppz is generally better protected from water in the Δ-enantiomer.

Figure 3 shows the equivalent data for Δ- and Λ-[Ru(phen)$_2$dppz]$^{2+}$ bound to [poly(dG-dC)]$_2$ (see also Tables S1 and S2 in the Supporting Information). There are notable differences in the shapes of the plots, but the most significant distinction is that Δ-[Ru(phen)$_2$dppz]$^{2+}$ does not follow the trend observed with [poly(dA-dT)]$_2$. Instead, the longer lifetime dominates at high [Nu]/[Ru] and the short lifetime grows-in as [Nu]/[Ru] decreases. Λ-[Ru(phen)$_2$dppz]$^{2+}$ does behave similarly with both alternating polynucleotides, but this is an exception. Λ–[Poly(dG-dC)]$_2$ differs not only from Δ–[poly(dG-dC)]$_2$, but also from all other dppz and methylated-dppz complexes we have studied with [poly(dG-dC)]$_2$.[28] The other notable difference is that for both enantiomers with [poly(dG-dC)]$_2$, the shift from predominance of one lifetime to the other occurs closer to the intercalation saturation point, and is sharper than observed with [poly(dA-dT)]$_2$. For both enantiomers, the long and short lifetimes with [poly(dG-dC)]$_2$ are smaller than those with [poly(dA-dT)]$_2$. However, with [poly(dG-dC)]$_2$, lifetimes for Δ- are only 70% higher than those for Λ-[Ru(phen)$_2$dppz]$^{2+}$, compared to 300% with [poly(dA-dT)]$_2$.

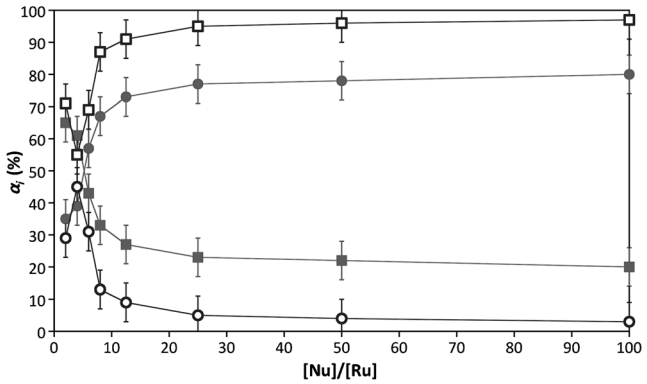

Figure 3. Pre-exponential factors (α_i) for enantiomers of [Ru(phen)$_2$dppz]$^{2+}$ bound to [poly(dG-dC)]$_2$ in phosphate buffer (5 mM, pH 6.9); Δ-enantiomer: closed symbols, τ_L=253(±6) ns (●), τ_S=71(±10) ns (■); Λ-enantiomer: open symbols, τ_L=138(±26) ns (○), τ_S=42(±4) ns (□); [Ru]=20 μM; λ_{ex}=440 nm; λ_{em}>540 nm.

The alternating co-polynucleotides are both B-form with dinucleotide steps, but have significant differences in secondary structure that can affect intercalation geometry and groove hydration. For example, the GC (three H bonds) intercalation pocket is deeper than the AT (two H bonds) pocket, and the minor groove in GC sequences is shallower and broader than that in AT sequences.[29] Replacing guanine by inosine gives [poly(dI-dC)]$_2$, which has a minor groove and intercalation pocket similar to [poly(dA-dT)]$_2$, but a major groove identical to [poly(dG-dC)]$_2$. This alteration results in lifetime and pre-exponential factor behaviour that is very similar to that observed with [poly(dA-dT)]$_2$ (Table 1). From this we conclude that shorter lifetimes are correlated with the presence of guanine, but at this stage we cannot distinguish whether it is a physical interaction with guanine or structural differences between polynucleotides (e.g., more shallow minor groove, deeper intercalation pocket of [poly(dG-dC)]$_2$) that are responsible.

Table 1. Emission of Δ-[Ru(phen)$_2$dppz]$^{2+}$ with alternating homo-polynucleotides.[a]

DNA	[Nu]/[Ru]	τ_L [ns]	α_L [%]	τ_S [ns]	α_S [%]
[poly(dA-dT)]$_2$	12.5	756	56	129	44
	50.0	737	26	135	74
[poly(dG-dC)]$_2$	12.5	254	73	61	27
	50.0	248	78	67	22
[poly(dI-dC)]$_2$	12.5	998	45	153	55
	50.0	912	25	160	75

[a] [Ru]=20 μM, phosphate buffer (5 mM, pH 6.9), 25 °C; λ_{ex}=440 nm, λ_{em}>540 nm; τ_i=emission lifetime, α_i=pre-exponential factor.

[Ru(phen)$_2$dppz]$^{2+}$ emission with non-alternating polynucleotides: DNA contains 16 base-pair steps, each with their own conformation and structure of intercalation pocket; some are symmetric, resulting in 12 unique steps (Figure 4).

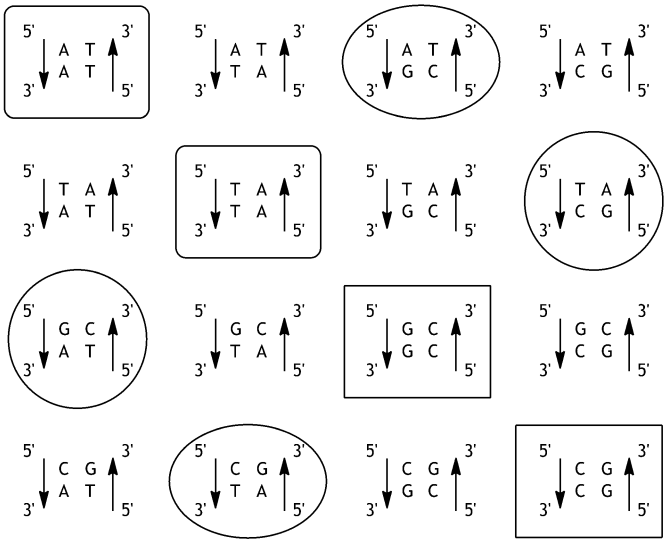

Figure 4. All possible base-pair steps in DNA. Equivalent steps are indicated by matching shapes. There are 12 non-equivalent steps.

**Poly(dA-dT)]$_2$ has two types of base-pair step [5′-A-T-3′]$_2$ and [5′-T-A-3′]$_2$. Likewise, [poly(dG-dC)]$_2$ has the steps [5′-G-C-3′]$_2$ and [5′-C-G-3′]$_2$. From our observation of double exponential decays at [Nu]/[Ru]=50 with homoduplexes [poly(dA)]·[poly(dT)] and [poly(dG)]·[poly(dC)], each with only one type of base-pair step, we previously concluded that the two lifetimes do not arise from intercalation at different base-pair steps.[18] Table 2 presents the binding-ratio dependence of [Ru(phen)$_2$dppz]$^{2+}$ enantiomer lifetimes with homoduplex [poly(dA)]·[poly(dT)] and [poly(dG)]·[poly(dC)], with triplex [poly(dT)]·[poly(dA)]·[poly(dT)] shown for comparison. Linear dichroism studies showed intercalation of [Ru(phen)$_2$dppz]$^{2+}$ with these polynucleotides.[30]

Table 2. Emission of $Ru(phen)_2dppz]^{2+}$ enantiomers with non-alternating homo-polynucleotides.[a]

DNA[b]	[Nu]/[Ru]	Δ-$[Ru(phen)_2dppz]^{2+}$				Λ-$[Ru(phen)_2dppz]^{2+}$			
		τ_L [ns]	α_L [%]	τ_S [ns]	α_S [%]	τ_L [ns]	α_L [%]	τ_S [ns]	α_S [%]
A·T	12.5	802	72	155	28	130	22	42	78
	50.0	796	59	168	41	181	10	43	90
G·C	12.5	174	38	51	62	320	25	70	75
	50.0	156	39	54	61	367	42	74	58
T-A·T	75.0	655	92	324	8	443	73	225	27

[a] [Ru] = 20 μM, phosphate buffer (5 mM, pH 6.9), 25 °C; λ_{ex} = 440 nm, λ_{em} > 540 nm; τ_i = emission lifetime, α_i = pre-exponential factor. [b] A·T = [poly(dA)]·[poly(dT)]; G·C = [poly(dG)]·[poly(dC)]; T-A·T = [poly(dT)]-[poly(dA)]·[poly(dT)].

Notably, for Λ-$[Ru(phen)_2dppz]^{2+}$, lifetimes are longer with [poly(dG)]·[poly(dC)] than with [poly(dA)]·[poly(dT)], and are also longer than those for Λ–$[poly(dG\text{-}dC)]_2$. In fact, the Λ–[poly(dG)]·[poly(dC)] lifetimes are the longest we observe for $[Ru(phen)_2dppz]^{2+}$ with any GC-polynucleotide, for either enantiomer. For the Δ-enantiomer, the lifetimes are longer with non-alternating AT duplex and triplex than with the alternating duplex. This is consistent with higher emission reported for the racemate with these polynucleotides.[17]

Since these polynucleotides have non-standard B-like conformations,[29] it would be unwise to draw analogies with binding to other DNA sequences. Undoubtedly, the intercalation pockets in these non-alternating polynucleotides are subtly, or even dramatically, different from those in alternating or random sequences. We must bear in mind that genomic DNA can contain stretches of non-alternating DNA, and that the photophysics of the complexes in mixed-sequence DNA will not solely reflect the lifetimes observed in exemplar alternating homopolymers.

$[Ru(bpy)_2dppz]^{2+}$ emission as a function of nucleic acid sequence: Our studies of electron transfer between Δ-$[Ru(phen)_2dppz]^{2+}$ and Δ-$[Rh(phi)_2bpy]^{2+}$ bound to $[poly(dA\text{-}dT)]_2$ suggested a small degree of self-cooperativity in the binding of Δ-$[Ru(phen)_2dppz]^{2+}$ complexes (but not Λ), although substantially less than the Rh/Ru cooperativity.[31] Models for nearest-neighbour intercalation of Δ-$[Ru(phen)_2dppz]^{2+}$ in the minor groove,[5,32] suggested potential overlap of the central phenanthroline rings for the Δ- but not the Λ-enantiomer as a source of cooperativity. To investigate whether the ancillary ligands gave rise to complex–complex interactions, phenanthroline was exchanged for bipyridine to eliminate the central ring and the possibility of van der Waals stacking.

In recent work,[23] we proposed a novel binding model for the enantiomers of $[Ru(phen)_2dppz]^{2+}$ and $[Ru(bpy)_2dppz]^{2+}$ with $[poly(dA\text{-}dT)]_2$, based on fits of calorimetric and photophysical data at moderate binding ratios. Here, we report the photophysics with alternating polynucleotides over an expanded binding ratio range. Figure 5 and Figure 6 (also Tables S3 and S4 in the Supporting Information) show the variation with [Nu]/[Ru] of the relative pre-exponential factors (α_i) for the long (τ_L) and short (τ_S) lifetime components for Δ- and Λ-$[Ru(bpy)_2dppz]^{2+}$ bound to, respectively, $[poly(dA\text{-}dT)]_2$ and $[poly(dG\text{-}dC)]_2$.

The variation of pre-exponential factors with binding ratio for both Λ-enantiomers with $[poly(dA\text{-}dT)]_2$ is almost identical, with about 90% of short lifetime at [Nu]/[Ru] = 100 (50 base pairs per complex). We see 100% of the short lifetime component for Δ-$[Ru(bpy)_2dppz]^{2+}$ with $[poly(dA\text{-}dT)]_2$ at this binding ratio, but only about 80% for Δ-$[Ru(phen)_2dppz]^{2+}$. With $[poly(dG\text{-}dC)]_2$, by contrast, the variation of pre-exponential factors with binding ratio is the same for both Δ-enantiomers, with about 80% of long lifetime at [Nu]/[Ru] = 100. For Λ-$[Ru(bpy)_2dppz]^{2+}$ there is about 95% long lifetime, whereas for Λ-$[Ru(phen)_2dppz]^{2+}$ there is about 95% short lifetime.

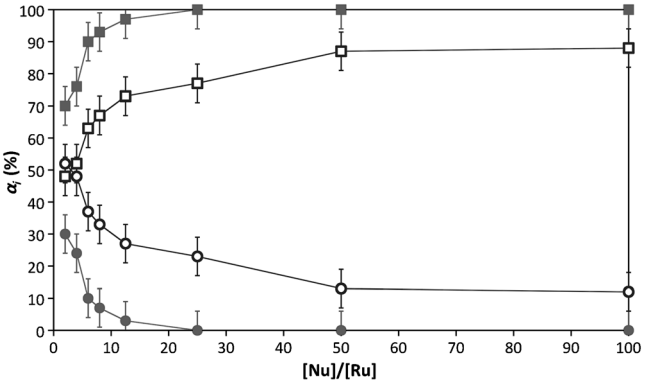

Figure 5. Pre-exponential factors (α_i) for enantiomers of $[Ru(bpy)_2dppz]^{2+}$ bound to $[poly(dA\text{-}dT)]_2$ in phosphate buffer (5 mM, pH 6.9); Δ-enantiomer: closed symbols, τ_L = 476(±63) ns (●), τ_S = 115(±10) ns (■); Λ-enantiomer: open symbols, τ_L = 267(±35) ns (○), τ_S = 38(±7) ns (□); [Ru] = 20 μM; λ_{ex} = 440 nm; λ_{em} > 540 nm.

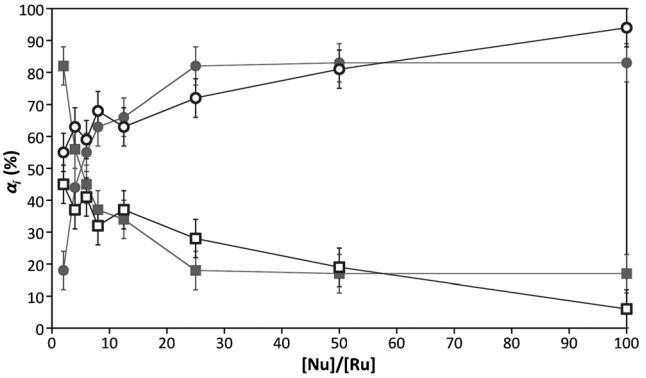

Figure 6. Pre-exponential factors (α_i) for enantiomers of $[Ru(bpy)_2dppz]^{2+}$ bound to $[poly(dG\text{-}dC)]_2$ in phosphate buffer (5 mM, pH 6.9); Δ-enantiomer: closed symbols, τ_L = 209(±14) ns (●), τ_S = 62(±14) ns (■); Λ-enantiomer: open symbols, τ_L = 63 ± (9) ns (○), τ_S = 32(±5) ns (□); [Ru] = 20 μM; λ_{ex} = 440 nm; λ_{em} > 540 nm.

Emission of dimeric $[Ru(phen)_2dppz]^{2+}$ with $[poly(dA\text{-}dT)]_2$: To further explore the origin of the double-exponen-

tial luminescence decays, dimeric complexes (Figure 1) were synthesised. These dimers were designed to bind as bis-intercalators with two base-pair separation of the intercalated dppz ligands, and linear dichroism spectra confirm that this occurs, as expected,[31] with both a C_4 and a C_2 linker. Like the monomers, the dimers are non-emissive in water and display double-exponential emission decays when bound to DNA. They also show evidence for two binding modes in preliminary calorimetry measurements (Figure S5 in the Supporting Information), for which the shape of the plot is similar to that observed for the monomer with [poly(dA-dT)]$_2$.[23] The decay parameters for the Δ-monomers and Δ,Δ-diastereoisomers of the C_4 and C_2 dimers bound to [poly(dA-dT)]$_2$ at [Nu]/[Ru] = 10 are compared in Table 3.

Table 3. Time-resolved emission of Δ-[Ru(L)$_2$dppz]$^{2+}$ monomers and Δ,Δ-[μ-c$_x$-(cdppz)$_2$(L)$_4$Ru$_2$]$^{4+}$ dimers (x = 2 or 4) with [poly(dA-dT)]$_2$ at [Nu]/[Ru] = 10.[a]

	L = phen				L = bpy			
	τ_L [ns]	α_L [%]	τ_S [ns]	α_S [%]	τ_L [ns]	α_L [%]	τ_S [ns]	α_S [%]
C_4 dimer	789	59	158	41	363	21	118	79
monomer[b]	732	59	134	41	476	5	115	95
C_2 dimer	489	28	153	72	194	46	86	54

[a] [Ru] = 20 μM, phosphate buffer (5 mM, pH 6.9), 25 °C; λ_{ex} = 440 nm, λ_{em} > 540 nm; τ_i = emission lifetime, α_i = pre-exponential factor. [b] For the monomeric complexes, the quoted lifetimes are the average values shown in Tables S1–S4 in the Supporting Information; pre-exponential factors are the mean of the values obtained at [Nu]/[Ru] = 8 and 12.5.

The similarity of the data for Δ,Δ-[μ-c$_4$(cdppz)$_2$-(phen)$_4$Ru$_2$]$^{4+}$ and Δ-[Ru(phen)$_2$dppz]$^{2+}$ under these conditions is striking. For the C_4-bpy analogue, similar decay as the monomer is observed instead at [Nu]/[Ru] = 4 (Tables S5–S7 in the Supporting Information). Complex Δ,Δ-[μ-c$_4$(cdppz)$_2$(bpy)$_4$Ru$_2$]$^{4+}$ has the same short lifetime as the monomer, but the long lifetime and pre-exponential factors are somewhat different. The data for the C_2 dimers show significant differences from those of the monomer. Thus, the linkers constrain the individual complexes in the dimers to bind with intercalation geometries that are different from those of the monomers.

Like the monomers, the lifetimes of the dimers are essentially independent of [Nu]/[Ru] for a given polynucleotide. However, the pre-exponential factors for the dimers are also relatively invariant, in contrast to the behaviour observed for the monomers. Table 4 illustrates this for Δ,Δ-[μ-c$_2$-(cdppz)$_2$(bpy)$_4$Ru$_2$]$^{4+}$ bound to [poly(dA-dT)]$_2$ as a function of binding ratio.

Table 4. Time-resolved emission of Δ,Δ-[μ-c$_2$(cdppz)$_2$(L)$_4$Ru$_2$]$^{4+}$ with [poly(dA-dT)]$_2$.[a]

[Nu]/[Ru]	L = phen				L = bpy			
	τ_L [ns]	α_L [%]	τ_S [ns]	α_S [%]	τ_L [ns]	α_L [%]	τ_S [ns]	α_S [%]
5	544	22	160	78	185[b]	49[b]	89[b]	51[b]
10	489	28	153	72	194	46	86	54
40	468	28	153	72	206	36	94	64
τ_{av} (±SD)	500 (39)	26 (3)	155 (4)	74 (3)	200 (8)	41 (7)	90 (6)	59 (7)

[a] [Ru] = 20 μM, phosphate buffer (5 mM, pH 6.9), 25 °C; λ_{ex} = 440 nm, λ_{em} > 540 nm; τ_i = emission lifetime, α_i = pre-exponential factor. [b] Values on initial mixing; after equilibration these changed to τ_L = 226 ns, α_L = 24, τ_S = 111 ns, α_S = 76.

[Ru(phen)$_2$dppz]$^{2+}$ emission quenching by nucleotides in DMF: One possible explanation for the lower emission lifetimes observed in [poly(dG-dC)]$_2$ compared to [poly(dA-dT)]$_2$ is that guanine physically quenches the [Ru(phen)$_2$dppz]$^{2+}$ emissive state. Photoinduced electron transfer from guanine to the excited state of a bound dye is a potential quenching mechanism that can be very efficient for intercalating organic dyes.[33] This is observed with [Ru(TAP)$_2$dppz]$^{2+}$[34] where electron transfer results in formation of [Ru(TAP)(TAP$^{\bullet-}$)dppz]$^{2+}$ and G$^{\bullet+}$. In [Ru(phen)$_2$dppz]$^{2+}$, the emissive ^{3}MLCT is based on the intercalated dppz ligand, so the product would be [Ru(phen)(dppz$^{\bullet-}$)]$^{2+}$.

We tested the hypothesis of guanine quenching by examining the quenching of Δ-[Ru(phen)$_2$dppz]$^{2+}$ by various nucleosides in an organic solvent, since the complex is non-emissive in water. DMF was identified as the only common solvent for which [Ru(phen)$_2$dppz]$^{2+}$ had a reasonably high emission quantum yield[8] and in which all the nucleosides dissolved at the concentrations required for quenching studies. No common non-aqueous solvent could be found for high concentrations of nucleoside monophosphate; thus, there are no electrostatic interactions between lumiphore and quencher in these studies. Furthermore, there were no indications of ground-state interactions between the species, so encounters between reactants are expected to be diffusion-limited.

Figure 7 shows that, of the bases contained in the polynucleotides, only guanine significantly quenches [Ru(phen)$_2$dppz]$^{2+}$ emission. Inosine does not quench the emission; this supports the hypothesis that the shorter lifetimes in [poly(dG-dC)]$_2$ result from physical quenching of the ^{3}MLCT by guanine. For guanine, the lifetime and intensity are equally (and linearly) quenched, which indicates absence of static quenching. However, the quenching rate constant with 2′-deoxyguanosine, $k_q = 2\times10^8\,M^{-1}s^{-1}$, is an order of magnitude lower than the calculated diffusion-controlled limit in DMF (see the Supporting Information).

The likely mechanism for quenching is electron transfer from guanine to *[Ru(phen)$_2$dppz]$^{2+}$, although this awaits transient spectroscopic confirmation. The free energy estimated for this electron transfer reaction predicts unfavourable energetics for all nucleosides, but the driving force for reduction by 2′-dG is >500 mV greater than that of the other nucleosides (see the Supporting Information). However, the exact magnitudes of the base potentials are always subject to question due to the difficulty of measuring the relevant redox potential in spectroscopic solvents; thus requiring corrections to be applied. Hence, the uncertainty in calculating free en-

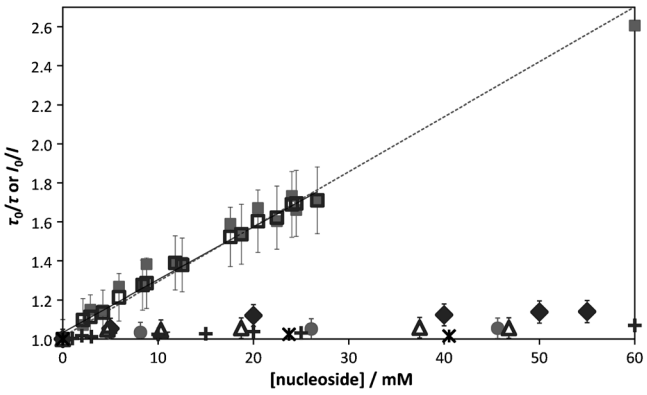

Figure 7. Stern–Volmer plot for quenching of Δ-*$[Ru(phen)_2dppz]^{2+}$ by 2′-deoxynucleosides in DMF; dG (*I*: ■; *τ*: □); dA (●); dC (◆); dT (△); dI (+); ribose (✱); [Ru] = 10 μM; 20 °C.

ergies for electron-transfer reactions involving DNA bases can be large.

Discussion

We have recently developed a novel model for the binding of $[Ru(L)_2dppz]^{2+}$ to $[poly(dA\text{-}dT)]_2$ (where L = phen or bpy) based on multivariate simultaneous fitting of calorimetry and photophysics data.[23] Figure 8 summarises the main features of the model.

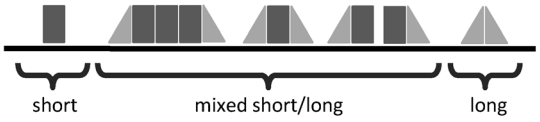

Figure 8. Summary of binding model for $[Ru(L)_2dppz]^{2+}$ to $[poly(dA\text{-}dT)]_2$ from Andersson et al.[23] Other combinations of binding modes cannot be sterically accommodated in B-DNA. Squares represent the symmetric intercalation mode, and triangles represent the left- and right-canted intercalation modes.

Two types of intercalative binding from the minor groove are proposed for $[Ru(L)_2dppz]^{2+}$. In the *symmetric mode*, the long axis of the dppz ligand lies perpendicular to the long axis of the base pairs. In the *canted mode*, the long dppz axis lies about 30° away from perpendicular; the complex can be canted to the left or the right, depending on its environment and neighbours. Both these geometries have been observed, at different intercalation sites, in the recent crystal structure of $[Ru(phen)_2dppz]^{2+}$ with self-complementary decamer oligonucleotides.[25]

For intercalation with $[poly(dA\text{-}dT)]_2$, the long-lifetime component of emission is assigned to the canted geometry where one phenazine nitrogen is embedded in the pocket and the other exposed to water in the major groove. The short lifetime component is assigned to the symmetric intercalation geometry, where both phenazine nitrogen atoms are partially exposed to water in the major groove. The symmetric mode occurs for binding of isolated complexes and within contiguously bound stretches. Canted intercalation occurs, to the left and right, at either end of contiguous stretches of two or more complexes. Examples of sterically allowed arrangements are shown in Figure 8, along with the lifetime distributions expected for each arrangement. The actual arrangements that occur are dictated by a subtle interplay of repulsive complex–complex and attractive complex–DNA interactions, mediated by allosteric changes in the DNA. Fitting of calorimetric and photophysical data led to the conclusion that Δ-$[Ru(bpy)_2dppz]^{2+}$ prefers to bind as isolated complexes, due to anti-cooperative interactions with all neighbours. The other complexes have a mixture of cooperative and anti-cooperative interactions: Δ-$[Ru(phen)_2dppz]^{2+}$ has some preference for duplets of canted complexes, and the Λ-enantiomers bind as mixed arrangements but all complexes are reluctant to form consecutive stretches of more than three complexes.

These different types of binding produce differently shaped curves for the variation of pre-exponential factor with [Nu]/[Ru]. Preference for isolated binding gives a high percentage of one lifetime at [Nu]/[Ru] = 100, and little change in that percentage until [Nu]/[Ru] drops below 20. Preference for mixed binding gives a lower percentage of one lifetime at [Nu]/[Ru] = 100, and consistent change in that percentage as [Nu]/[Ru] drops. The precise shape and gradient of change depends on the relative strengths of cooperative and anti-cooperative interactions in the system; for example, the shape obtained for canted duplet preference is that observed for Δ-$[Ru(phen)_2dppz]^{2+}$ in Figure 2.

Binding of the dimeric complexes provides a prime example of what is expected when two complexes are constrained to always intercalate in nearest-neighbour sites. The similarity of the emission decay for Δ-$[Ru(phen)_2dppz]^{2+}$ and its C_4-dimer analogue at [Nu]/[Ru] = 10 is consistent with this dimer binding as duplets of canted complex. The congruence of the emission decay for Δ-$[Ru(bpy)_2dppz]^{2+}$ and its C_4-dimer analogue at [Nu]/[Ru] = 4 indicates that this dimer has a mixed symmetric/canted intercalation mode, which is amenable to forming contiguous closely-packed series. That the C_2-dimer analogue has different lifetimes as well as pre-exponential factors indicates that the shorter linker chain in the major groove causes substantially different binding of this molecule.

From the $[poly(dG\text{-}dC)]_2$ data in Figures 3 and 6, some conclusions about binding can be drawn from the shapes of the curves, even without assignment of the short and long lifetimes to specific intercalation geometries. Λ-$[Ru(phen)_2dppz]^{2+}$ clearly has a preference for binding in isolated sites, with dominance of the short lifetime component. Λ-$[Ru(bpy)_2dppz]^{2+}$ shows highly cooperative behaviour that produces a strongly inclined curve, with dominance of the long lifetime component. The Δ-enantiomers display mixed binding but with low gradients, implying that the preferred binding mode is anti-cooperative to other interactions. There is little effect of ancillary ligand on the Δ-enantiomer interaction with $[poly(dG\text{-}dC)]_2$, as previously observed for

the Λ-enantiomer with $[poly(dA\text{-}dT)]_2$. This suggests that the binding geometries of the enantiomers are somewhat different in $[poly(dG\text{-}dC)]_2$, so that ligand–ligand interactions in the groove are less important, but ligand–backbone interactions are more important than in $[poly(dA\text{-}dT)]_2$.

In order to assign lifetimes to different binding geometries for $[poly(dG\text{-}dC)]_2$, we refer to the recent crystal structures for binding of Λ-$[Ru(TAP)_2dppz]^{2+}$[24] and Λ-$[Ru(phen)_2dppz]^{2+}$[25] with oligonucleotides. In both structures, canted intercalation is observed at "non-classical" base-pair steps involving GC base pairs, in the former at a terminal 5′-G-A-3′ step with a flipped-out adenine, in the latter at a terminal 5′-G-G-3′ step with a *syn* conformation of the terminal G. Interestingly, NMR structures for related DNA-bound complexes—$[Ru(Me_2phen)dppz]^{2+}$[26] and $[Ru(tpm)(dppz)(py)]^{2+}$[27]—have also shown intercalation at 5′-G-A-3′ steps, but with indications of binding heterogeneity. Cartoons that show symmetric and canted binding at unperturbed $(AT)_2$ and $(GC)_2$ steps are shown in Figure 9. The observed stacking interactions give an indication of the possible positions of the phenazine nitrogen atoms with respect to the grooves and their associated water molecules. Because the ruthenium is displaced further from the helix axis in GC-rich sites, the positions of the nitrogen atoms in both geometries are shifted with respect to AT-rich sites. It appears that both symmetric and canted geometries in $[poly(dG\text{-}dC)]_2$ should give somewhat better protection from water in the major groove, but in the absence of structural information or MD simulations for all intercalation sites, it is difficult to predict which geometry has the greatest exposure to water.

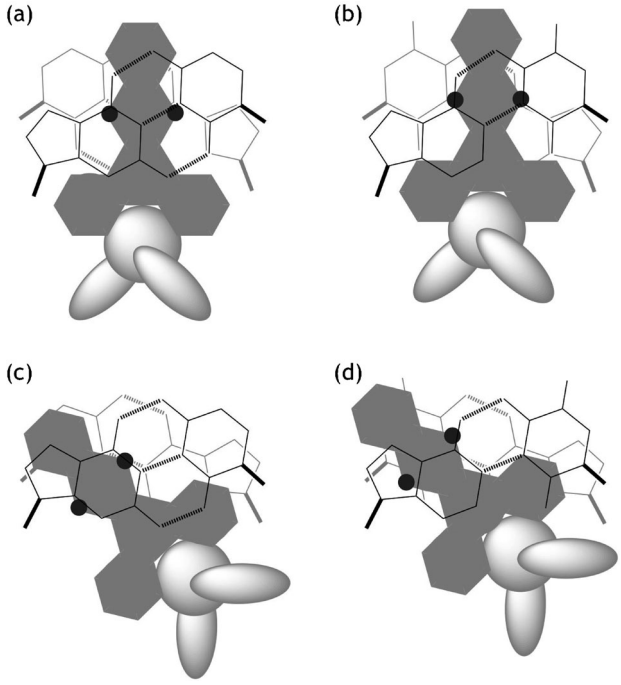

Figure 9. Cartoons to compare: a), b) symmetric, and c), d) canted intercalation of Δ-$[Ru(L)_2dppz]^{2+}$ at $(GC)_2$ (a, c) and $(AT)_2$ (b, d) steps.

In the crystal structure of Λ-$[Ru(phen)_2dppz]^{2+}$,[25] symmetric intercalation is observed at a central 5′-T-A-3′ step with exposure of both dppz nitrogen atoms to the major groove. For symmetric intercalation in $[poly(dG\text{-}dC)]_2$, both nitrogen atoms are withdrawn towards the centre of the intercalation pocket as the ruthenium is displaced further from the helix axis. Depending on the displacement distance, both those nitrogen atoms could become protected within the intercalation pocket, making the lifetime longer than that geometry in $[poly(dA\text{-}dT)]_2$. If both nitrogen atoms are protected in the canted geometry with $[poly(dA\text{-}dT)]_2$, then displacement of the ruthenium centre in $[poly(dG\text{-}dC)]_2$ could expose one of the nitrogen atoms to the minor groove. Indeed, this appears to be the case for the canted geometry observed at a $(GC)_2$ site in the crystal structure.[25] A photophysical model based on these features would assign the long lifetime in $[poly(dG\text{-}dC)]_2$ to symmetric intercalation and the short lifetime to canted intercalation. The variation of pre-exponential factors with binding ratio, which is generally inverted with $[poly(dG\text{-}dC)]_2$ compared to $[poly(dA\text{-}dT)]_2$, is then consistent with the isolated/adjacently bound complex model (Figure 8). Of course, the Δ- and Λ-enantiomers can be different in their binding geometries and photophysics, depending on the accessibility of the nitrogen atoms to water molecules in the grooves of DNA.

Since both lifetimes with $[poly(dG\text{-}dC)]_2$ are significantly shorter than observed with $[poly(dA\text{-}dT)]_2$, quenching by guanine may also make an important contribution, as observed in DMF with the nucleoside. Therefore, we cannot exclude the possibility that the canted geometry has an intrinsically longer lifetime but is quenched more efficiently than the symmetric geometry, so that the observed lifetime for the former geometry becomes the shorter one. On-going calorimetric, structural, transient spectroscopy and molecular dynamics studies should help distinguish between these two possibilities and allow absolute assignment of the intercalation geometries in $[poly(dG\text{-}dC)]_2$ and other DNA sequences.

Conclusion

The Δ- and Λ-enantiomers of $[Ru(L)_2dppz]^{2+}$ must be considered as individual species with their own distinct photophysical and binding properties when they interact with the chiral environment of nucleic acids. Moreover, the photophysics of each bound enantiomer of $[Ru(L)_2dppz]^{2+}$ depend strongly on the sequence and conformation of the nucleic acid. Small variations in ancillary ligand cause significant differences in luminescence lifetimes and amplitudes for the bound dyes. Generally, two lifetimes are observed when any enantiomer of $[Ru(L)_2dppz]^{2+}$ binds to double-stranded DNA, and the magnitudes of the lifetimes and pre-exponential factors are very sensitive to nucleic acid sequence and conformation, as well as enantiomer.

The lifetimes and pre-exponential factors are also sensitive to the nature of the ancillary ligand, even if the change is apparently small as when changing between L = phen or bpy. The magnitude and direction of variations in τ_i and α_i depend on the sequence of the DNA. Thus, with [poly(dA-dT)]$_2$, the variation of α_i with [Nu]/[Ru] has little dependence on L for Λ-$[Ru(L)_2dppz]^{2+}$, but a substantial dependence for Δ-$[Ru(L)_2dppz]^{2+}$. However, with [poly(dG-dC)]$_2$, it is the Λ-enantiomer α_i values that depend strongly on the nature of L, whereas those of the Δ-enantiomer are relatively unaffected.

According to the model developed by Andersson et al.[23] to correlate enthalpy changes and luminescence pre-exponential factors, the two lifetimes are related to different geometries of $[Ru(L)_2dppz]^{2+}$ intercalated from the minor groove. In [poly(dA-dT)]$_2$, canted and symmetric binding geometries of the dppz ligand give rise to, respectively, the long and short lifetimes as a result of differential exposure of the dppz nitrogen atoms to water in the grooves. The symmetric geometry occurs for isolated bound complexes and those within a contiguous sequence. The canted geometries occur at either end of contiguous sequences. It is likely that similar geometries are responsible for the two lifetimes with [poly(dG-dC)]$_2$, but it appears that the geometry for isolated molecules generally results in the longer lifetime in this environment, as a consequence of lower dppz exposure to water in the symmetric geometry. The significantly shorter lifetimes observed in [poly(dG-dC)]$_2$ may also arise from electron transfer to the $[Ru(L)_2dppz]^{2+}$ emissive state from guanine. Therefore, there remains a possibility that the canted geometry has an intrinsically longer lifetime but is quenched more efficiently than the symmetric geometry, so that the observed lifetime for the former geometry becomes the shorter one.

Experimental Section

Enantiomers of $[Ru(phen)_2dppz]Cl_2$ and $[Ru(bpy)_2dppz]Cl_2$ were prepared and purified as previously described,[12,23,35] and solutions were prepared in HPLC-grade water. Excitation spectroscopy was used to establish that emissive ruthenium complex impurities made up $<0.1\%$ of each sample. Enantiomeric purity was established by CD spectroscopy (Jasco J-720). The concentrations of $[Ru(phen)_2dppz]^{2+}$ and $[Ru(bpy)_2dppz]Cl_2$ in HPLC-grade water were determined by using $\varepsilon_{440\,nm} = 20000\,M^{-1}cm^{-1}$[12] and $16100\,M^{-1}cm^{-1}$,[9] respectively. Dimeric complex Δ,Δ-$[\mu\text{-}c_4(cdppz)_2(phen)_4Ru_2]Cl_4$, was prepared as described elsewhere[19] and its concentration in water was also determined by using $\varepsilon_{440\,nm} = 20000\,M^{-1}cm^{-1}$ per ruthenium unit since no stacking was observed.

Synthetic polydeoxyribonucleotides [poly(dA-dT)]$_2$, [poly(dG-dC)]$_2$, [poly(dI-dC)]$_2$, [poly(dA)]·[poly(dT)], [poly(dG)]·[poly(dC)] were from Amersham-Pharmacia (now GE Healthcare). All commercial nucleic acid samples were supplied as lyophilised solids and were dissolved in HPLC-grade water. To remove excess salts, the solutions were dialysed extensively against HPLC-grade water, and ultimately dialysed against sodium phosphate buffer (5 mM, pH 6.9) for storage. Dry SpectraPor-2 dialysis tubing (Spectrum) with a suitable MWCO was treated with hot EDTA, and extensively washed in hot HPLC-grade water prior to use, to remove bound metal ions and organic impurities that might interfere with the photophysical experiments. Turbid DNA samples were filtered through 0.8 μm Millpore filters before storage. Nucleic acid concentrations were determined by using the extinction coefficients provided by the manufacturer; stated concentrations are those of nucleotide repeat units: [poly(dA-dT)]$_2$, $\varepsilon_{262\,nm} = 6600\,M^{-1}cm^{-1}$; [poly(dG-dC)]$_2$, $\varepsilon_{254\,nm} = 8400\,M^{-1}cm^{-1}$; [poly(dI-dC)]$_2$, $\varepsilon_{251\,nm} = 6900\,M^{-1}cm^{-1}$; [poly(dG)]·[poly(dC)], $\varepsilon_{253\,nm} = 7400\,M^{-1}cm^{-1}$; [poly(dA)]·[poly(dT)], $\varepsilon_{260\,nm} = 6000\,M^{-1}cm^{-1}$. Mononucleotides (Sigma) were of the highest available purity ($>99\%$) and were used as provided.

Concentrations of mononucleotide solutions prepared in organic solvents were determined by >100-fold dilution in HPLC-grade water by using the following extinction coefficients in aqueous solution: 2′-dG, $\varepsilon_{252\,nm} = 14230\,M^{-1}cm^{-1}$; 2′-dC, $\varepsilon_{271\,nm} = 8860\,M^{-1}cm^{-1}$; 2′-dA, $\varepsilon_{259\,nm} = 15080\,M^{-1}cm^{-1}$; 2′-dT, $\varepsilon_{267\,nm} = 9490\,M^{-1}cm^{-1}$; 2′-dI, $\varepsilon_{248\,nm} = 12300\,M^{-1}cm^{-1}$

Absorption spectra were measured with a Cary 100-Bio UV/Vis spectrometer. Emission and excitation spectra were recorded with a SPEX Fluoromax spectrofluorimeter. Emission lifetimes were determined by the frequency modulation method by using a SPEX Fluorolog-tau instrument; broadband emission was detected by using a high-pass filter for $\lambda > 540$ nm. For chosen samples, comparable results were obtained by single-photon counting with detection at the maximum emission wavelength.

The SPEX Fluorolog-tau reports the relative luminescence amplitude (f_i) for each lifetime (τ_i), which is converted to relative pre-exponential factor (α_i) by using the following expressions:[36]

$$I(t) = I_0[\alpha_1 \exp(-t/\tau_1) + \alpha_2 \exp(-t/\tau_2)]$$

where:

$$\alpha_i = \frac{f_i/\tau_i}{\sum f_i/\tau_i}$$

Experiments with polynucleotides were generally performed at low ionic strength in water to maximise electrostatic interactions of the ruthenium complexes with the nucleic acids, and to avoid any aggregation of complex that might occur at high ionic strength. The standard buffer was sodium phosphate (5 mM, pH 6.9) in HPLC-grade water.

Acknowledgements

EMT gratefully acknowledges the EU Marie Curie Fellowship programme, NFR, EPSRC (GR/S23315/01), and COST D35 for financial support for the research and networking that made this work possible. A.W.M. acknowledges receipt of an EPSRC DTA studentship from Newcastle University School of Chemistry. P.L. acknowledges funding from The Swedish Research Council (VR). The authors are exceedingly grateful to Prof. Christine Cardin for early communication of structural information.

[1] S. Campagna, F. Puntoriero, F. Nastasi, G. Bergamini, B. Balzani, *Top. Curr. Chem.* **2007**, *280*, 117–214.
[2] M. R. Gill, J. A. Thomas, *Chem. Soc. Rev.* **2012**, *41*, 3179–3192.
[3] J. K. Barton, E. D. Olmon, P. A. Sontz, *Coord. Chem. Rev.* **2011**, *255*, 619–634.
[4] H. J. Farrer, L. Salassa, P. J. Sadler, *Dalton Trans.* **2009**, 10690–10701.
[5] A. W. McKinley, P. Lincoln, E. M. Tuite, *Coord. Chem. Rev.* **2011**, *255*, 2676–2692.
[6] E. J. C. Olson, D. Hu, A. Hormann, A. M. Jonkman, M. R. Arkin, E. D. A. Stemp, J. K. Barton, P. F. Barbara, *J. Am. Chem. Soc.* **1997**, *119*, 11458–11467.
[7] E. Amouyal, A. Homsi, J.-C. Chambron, J.-P. Sauvage, *J. Chem. Soc. Dalton Trans.* **1990**, 1841–1845.
[8] R. B. Nair, B. M. Callum, C. J. Murphy, *Inorg. Chem.* **1997**, *36*, 962–965.

[9] J.-C. Chambron, J.-P. Sauvage, *Chem. Phys. Lett.* **1991**, *182*, 603–607.
[10] X.-Q. Guo, F. N. Castellano, L. Li, J. R. Lakowicz, *Biophys. Chem.* **1998**, *71*, 51–62.
[11] A. E. Friedman, J.-C. Chambron, J.-P. Sauvage, N. J. Turro, J. K. Barton, *J. Am. Chem. Soc.* **1990**, *112*, 4960–4962.
[12] C. Hiort, P. Lincoln, B. Nordén, *J. Am. Chem. Soc.* **1993**, *115*, 3448–3454.
[13] M. K. Brennaman, J. H. Alstrum-Acevedo, C. N. Fleming, P. Jang, T. J. Meyer, J. M. Papanikolas, *J. Am. Chem. Soc.* **2002**, *124*, 15094–15098.
[14] M. K. Brennaman, T. J. Meyer, J. M. Papanikolas, *J. Phys. Chem. A* **2004**, *108*, 9938–9944.
[15] B. Önfelt, J. Olofsson, P. Lincoln, B. Nordén, *J. Phys. Chem. A* **2003**, *107*, 1000–1009.
[16] J. Olofsson, B. Önfelt, P. Lincoln, *J. Phys. Chem. A* **2004**, *108*, 4391–4398.
[17] Y. Jenkins, A. E. Friedman, N. J. Turro, J. K. Barton, *Biochemistry* **1992**, *31*, 10809–10816.
[18] E. Tuite, P. Lincoln, B. Nordén, *J. Am. Chem. Soc.* **1997**, *119*, 239–240.
[19] J. Onfelt, P. Lincoln, B. Nordén, J. S. Baskin, A. H. Zewail, *Proc. Natl. Acad. Sci. USA* **2000**, *97*, 5708–5713.
[20] B. Olofsson, B. Önfelt, P. Lincoln, B. Nordén, P. Matousek, A. W. Parker, E. Tuite, *J. Inorg. Biochem.* **2002**, *91*, 286–297.
[21] C. Coates, J. Olofsson, M. Coletti, J. J. McGarvey, B. Önfelt, P. Lincoln, B. Nordén, E. M. Tuite, P. Matousek, A. W. Parker, *J. Phys. Chem. B* **2001**, *105*, 12653–12664.
[22] R. M. Hartshorn, J. K. Barton, *J. Am. Chem. Soc.* **1992**, *114*, 5919–5925.
[23] a) J. Andersson, PhD Thesis, Chalmers University of Technology, Sweden, 2012; b) J. Andersson, L. Fornander, M. Abrahamsson, E. Tuite, P. Nordell, P. Lincoln, *Inorg. Chem.* **2012**.
[24] J. P. Hall, K. O'Sullivan, A. Naseer, J. A. Smith, J. M. Kelly, C. J. Cardin, *Proc. Natl. Acad. Sci. USA* **2011**, *108*, 17610–17614.
[25] H. Niyazi, J. P. Hall, K. O'Sullivan, G. Winter, T. Sorensen, J. M. Kelly, C. J. Cardin, *Nature Chem.* **2012**, *4*, 621–628.
[26] A. Greguric, I. D. Greguric, T. W. Hambley, J. R. Aldrich-Wright, J. C. Collins, *J. Chem. Soc. Dalton Trans.* **2002**, 849–855.
[27] P. Waywell, V. Gonzalez, M. R. Gill, H. Adams, A. J. H. M. Meijer, M. P. Williamson, J. A. Thomas, *Chem. Eur. J.* **2010**, *16*, 2407–2417.
[28] A. W. McKinley, PhD Thesis, University of Newcastle upon Tyne, UK **2008**.
[29] a) V. A. Bloomfield, D. M. Crothers, I. Tinoco, Jr., *Nucleic Acids: Structures, Properties, and Functions*, University Science Books, **2000**; b) *Nucleic Acids in Chemistry and Biology* (Eds.: G. M. Blackburn, M. J. Gait, D. Loakes), 3rd ed., RSC, **2006**; c) S. Neidle, *Nucleic Acid Structure and Recognition*, Oxford University Press, **2002**.
[30] S.-D. Choi, M.-S. Kim, S. K. Kim, P. Lincoln, E. Tuite, B. Nordén, *Biochemistry* **1997**, *36*, 214–223.
[31] P. Lincoln, E. Tuite, B. Nordén, *J. Am. Chem. Soc.* **1997**, *119*, 1454–1455.
[32] B. Önfelt, P. Lincoln, B. Nordén, *J. Am. Chem. Soc.* **2001**, *123*, 3630–3637.
[33] G. D. Reid, D. J. Whittaker, M. A. Day, C. M. Creely, E. M. Tuite, J. M. Kelly, G. S. Beddard, *J. Am. Chem. Soc.* **2001**, *123*, 6953–6954.
[34] J. A. Smith, M. W. George, J. M. Kelly, *Coord. Chem. Rev.* **2011**, *255*, 2666–2675.
[35] P. Lincoln, B. Nordén, *J. Phys. Chem. B* **1998**, *102*, 9583–9594.
[36] J. R. Lakowicz, *Principles of Fluorescence Spectroscopy*, 2nd ed., Springer, **1999**.

Received: April 15, 2012
Published online: October 5, 2012

CHEMISTRY
A EUROPEAN JOURNAL

Supporting Information

DNA Sequence and Ancillary Ligand Modulate the Biexponential Emission Decay of Intercalated $[Ru(L)_2dppz]^{2+}$ Enantiomers

Andrew W. McKinley,[b] Johanna Andersson,[c] Per Lincoln,[c] and Eimer M. Tuite*[a]

chem_201201279_sm_miscellaneous_information.pdf

SUPPORTING INFORMATION

Original Figures in Colour
Figures 1-9

Additional Experimental Data
Tables S1-S7
Figures S1-S5

Additional Theory
Calculation of Diffusion-Controlled Rate Constant
Calculation of Driving Force for Photoinduced Electron Transfer

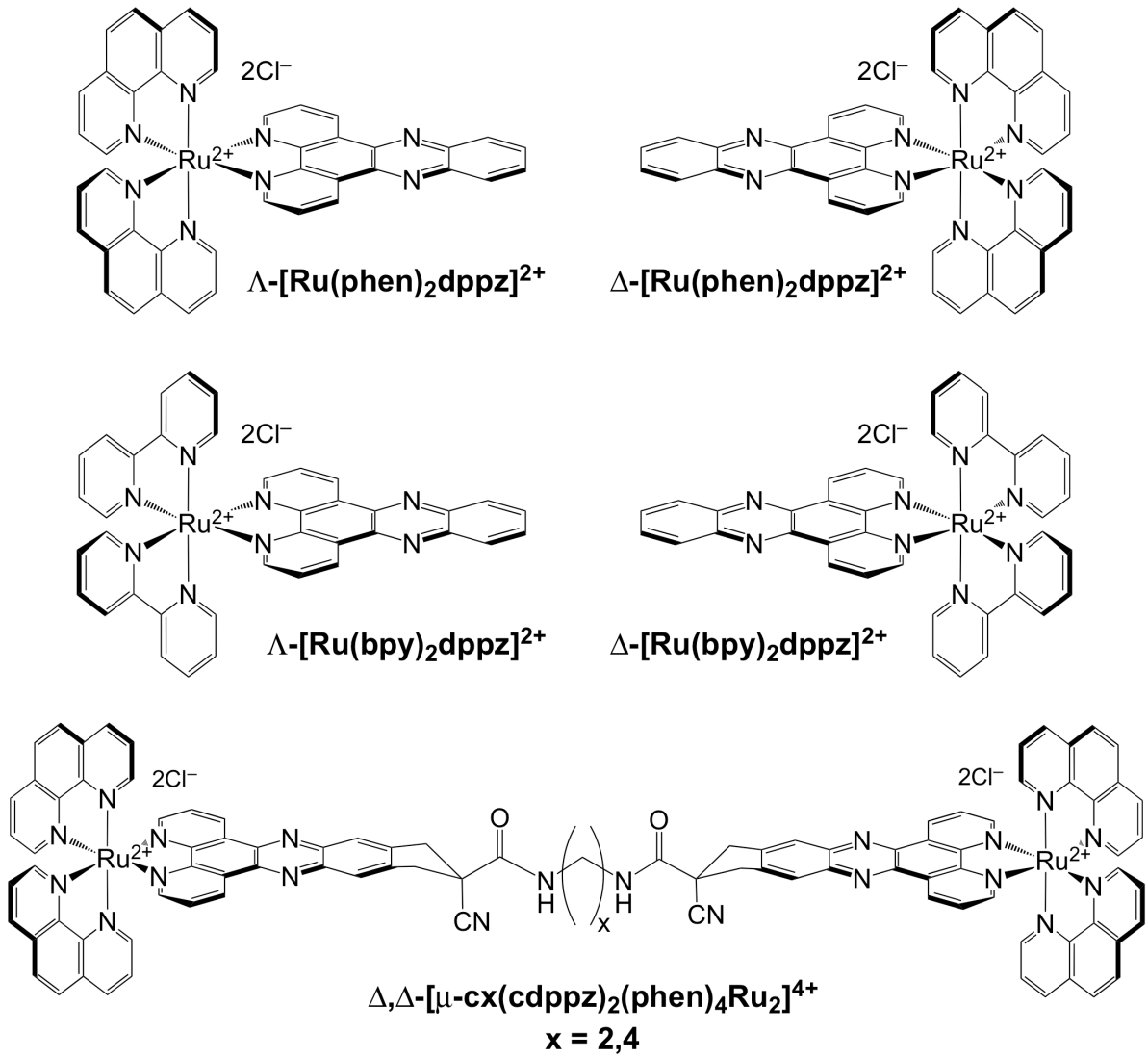

FIGURE 1. Structures of the studied complexes

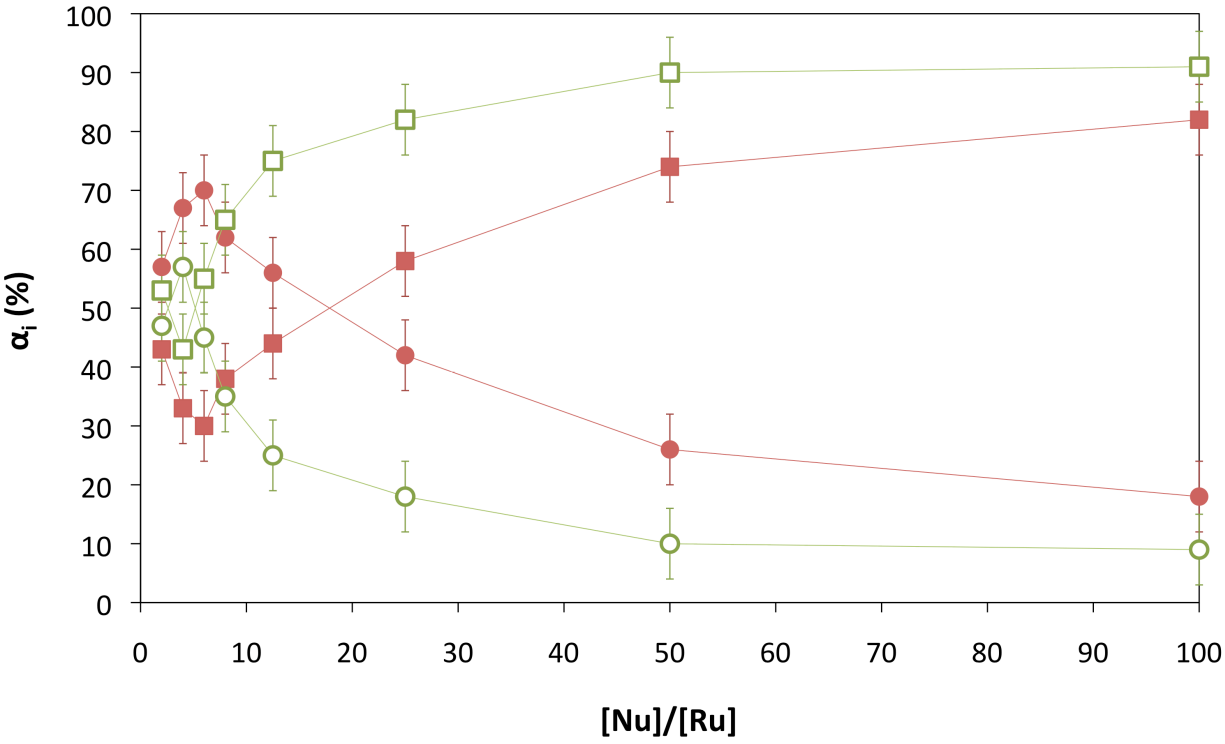

FIGURE 2. Pre-exponential factors (α_i) for enantiomers of $[Ru(phen)_2dppz]^{2+}$ bound to $[poly(dA\text{-}dT)]_2$ in 5 mM phosphate (pH 6.9) buffer. Δ- = closed symbols; τ_L = 732 (38) ns, ●; τ_S = 134 (10) ns, ■. Λ- = open symbols; τ_L = 327 (15) ns, ○; τ_S = 42 (6) ns, □. [Ru] = 20 μM. λ_{ex} = 440 nm; λ_{em} > 540 nm.

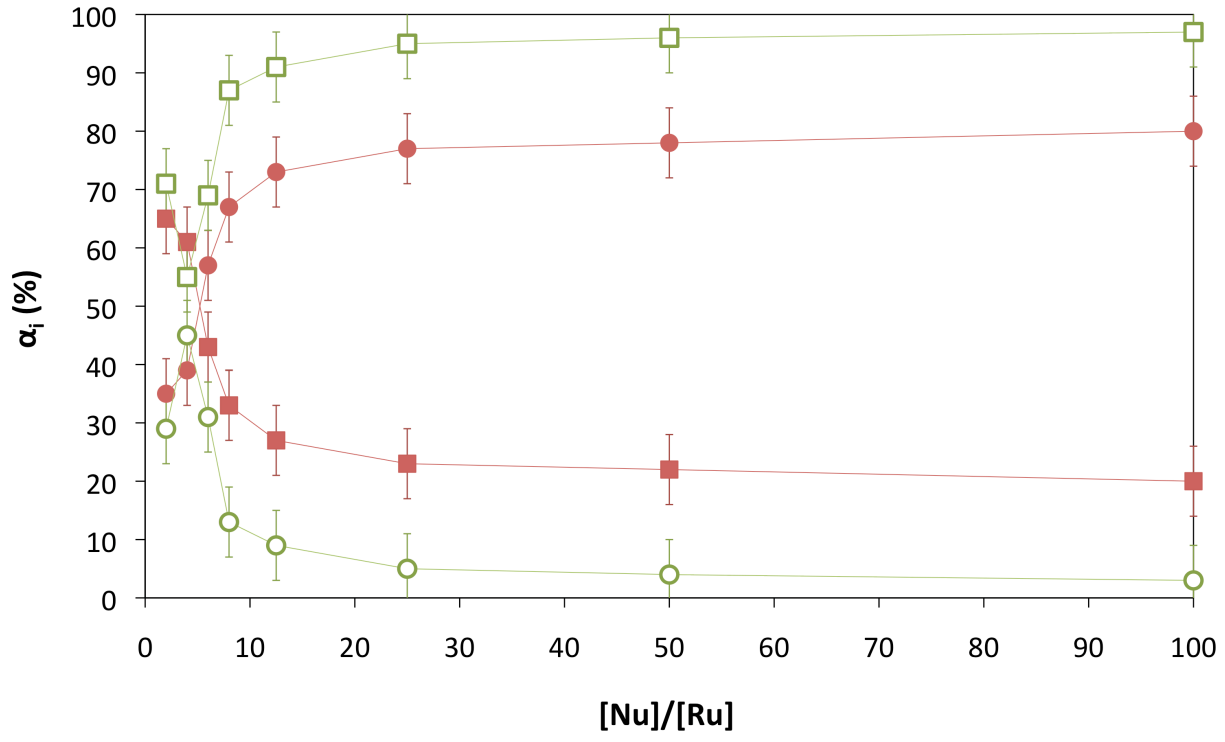

FIGURE 3. Pre-exponential factors (α_i) for enantiomers of $[Ru(phen)_2dppz]^{2+}$ bound to $[poly(dG\text{-}dC)]_2$ in 5 mM phosphate (pH 6.9) buffer. Δ- = closed symbols; τ_L = 253 (6) ns, ●; τ_S = 71 (10) ns, ■. Λ- = open symbols; τ_L = 138 (26) ns, ○; τ_S = 42 (4) ns, □. [Ru] = 20 μM. λ_{ex} = 440 nm; λ_{em} > 540 nm.

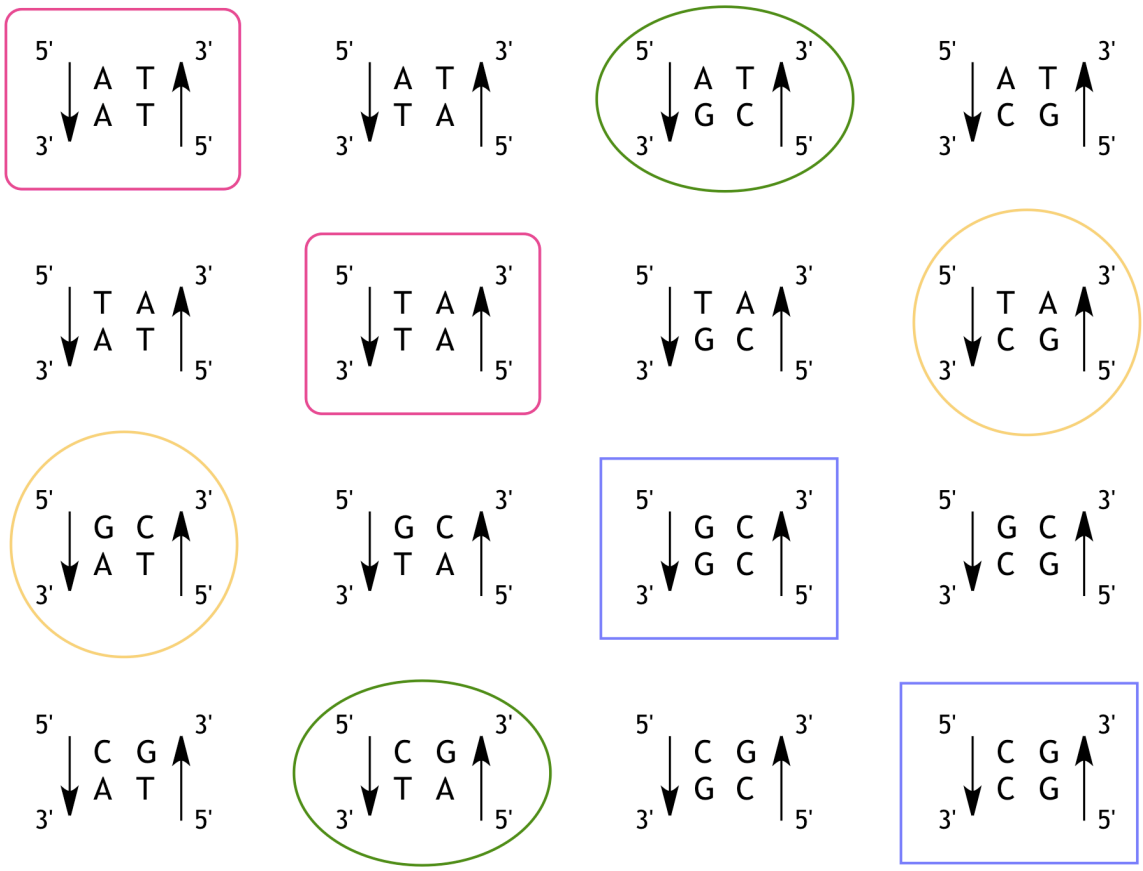

FIGURE 4. All possible basepair steps in DNA. Equivalent steps are indicated by identical highlight shapes. There are 12 non-equivalent steps.

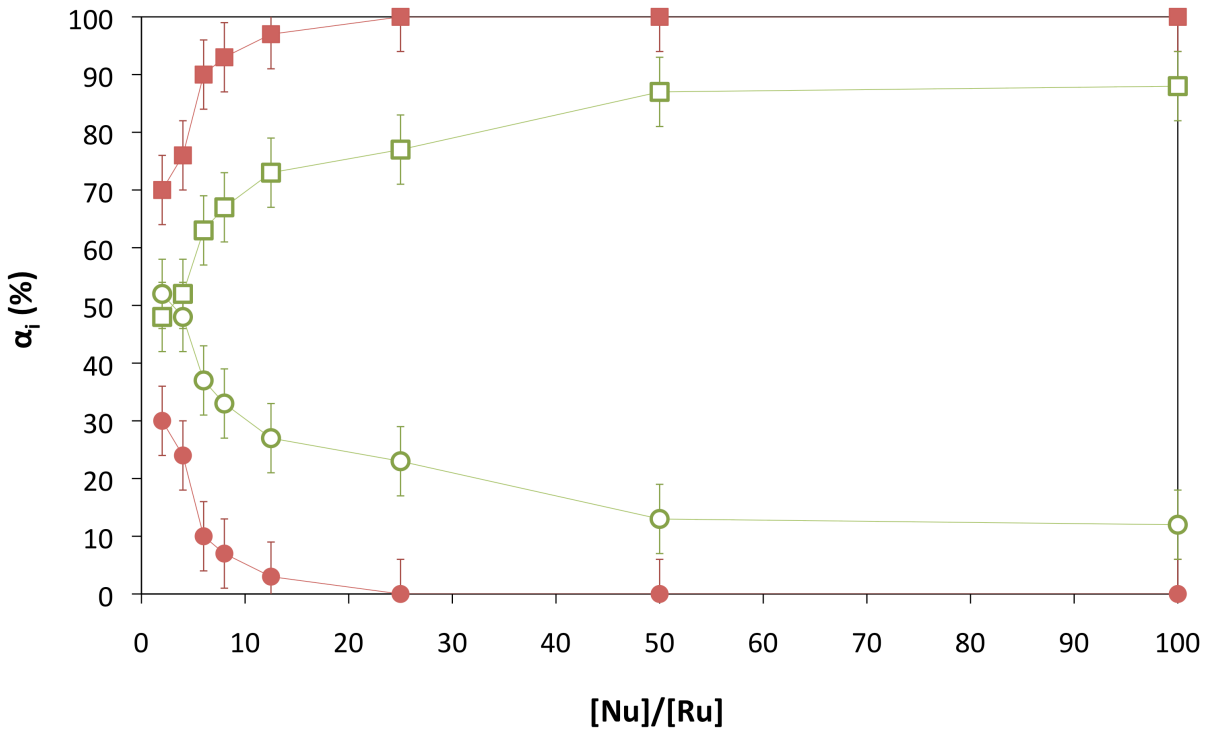

FIGURE 5. Pre-exponential factors (α_i) for enantiomers of $[Ru(bpy)_2dppz]^{2+}$ bound to $[poly(dA\text{-}dT)]_2$ in 5 mM phosphate (pH 6.9) buffer. Δ- = closed symbols; τ_L = 476 (63) ns, ●; τ_S = 115 (10) ns, ■. Λ- = open symbols; τ_L = 267 (35) ns, ○; τ_S = 38 (7) ns, □. [Ru] = 20 μM. λ_{ex} = 440 nm; λ_{em} > 540 nm.

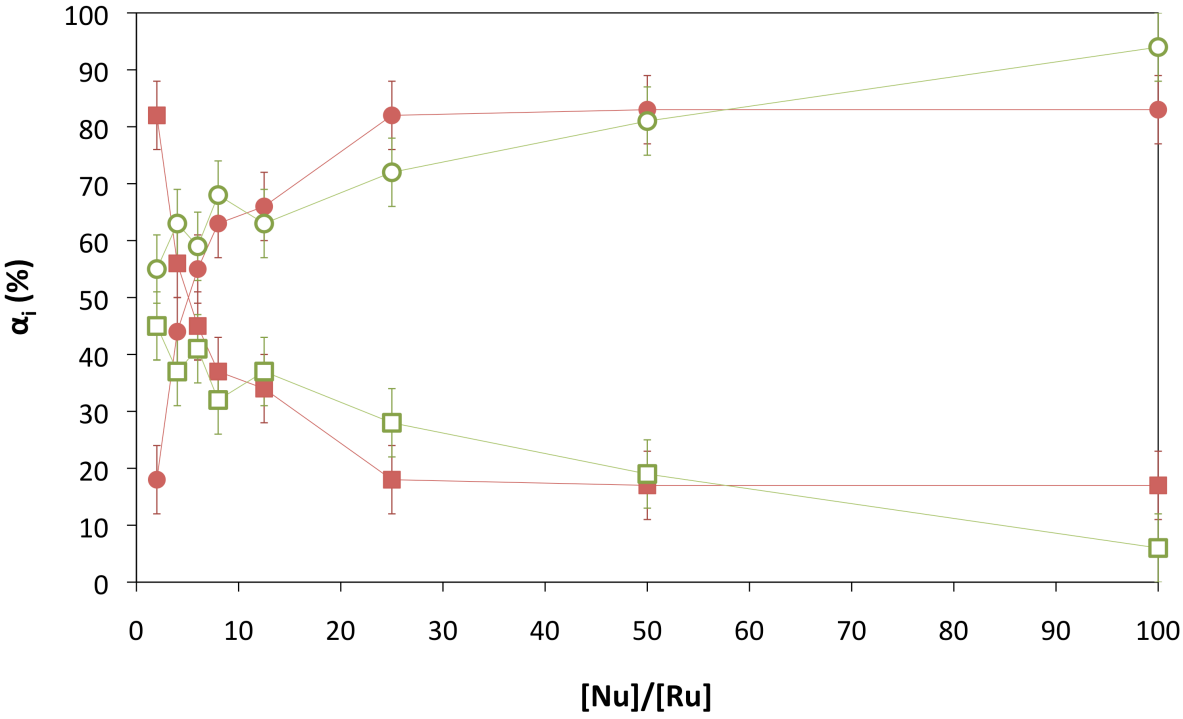

FIGURE 6. Pre-exponential factors (α_i) for enantiomers of $[Ru(bpy)_2dppz]^{2+}$ bound to $[poly(dG\text{-}dC)]_2$ in 5 mM phosphate (pH 6.9) buffer. Δ- = closed symbols; τ_L = 209 (14) ns, ●; τ_S = 62 (14) ns, ■. Λ- = open symbols; τ_L = 63 (9) ns, ○; τ_S = 32 (5) ns, □. [Ru] = 20 μM. λ_{ex} = 440 nm; λ_{em} > 540 nm.

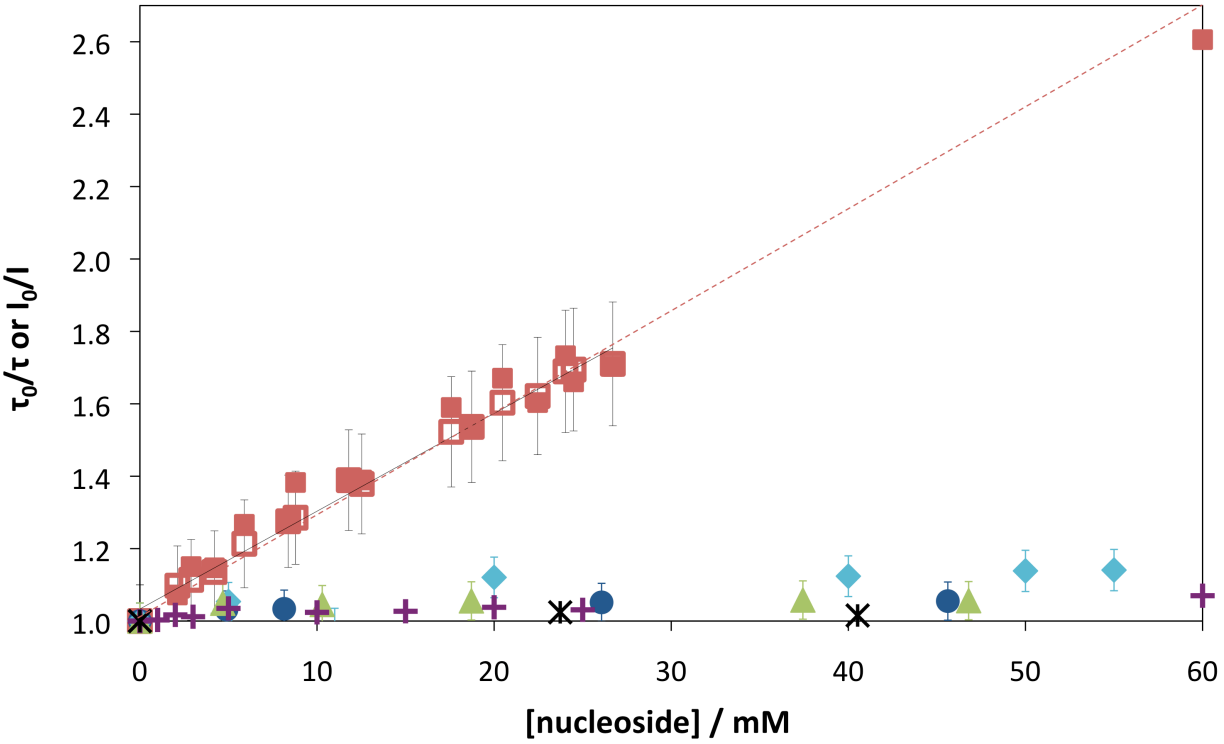

FIGURE 7. Stern-Volmer Plot for quenching of Δ-*[Ru(phen)$_2$dppz]$^{2+}$ by 2'-deoxynucleosides in DMF. dG (I, ■) (τ, □); dA (●); dC (◆); dT (▲); dI (+); ribose (∗). [Ru] = 10 μM; 20 °C.

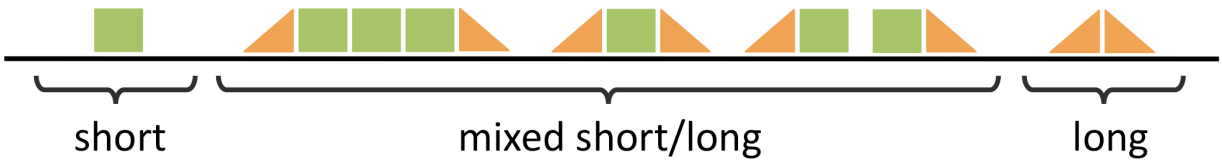

FIGURE 8. Summary of binding model for [Ru(L)$_2$dppz]$^{2+}$ to [poly(dA-dT)]$_2$ from Andersson *et al.*[23] Other combinations of binding modes cannot be sterically acccommodated in B-DNA. Squares represent the symmetric intercalation mode, and triangles represent the left- and right-canted intercalation modes.

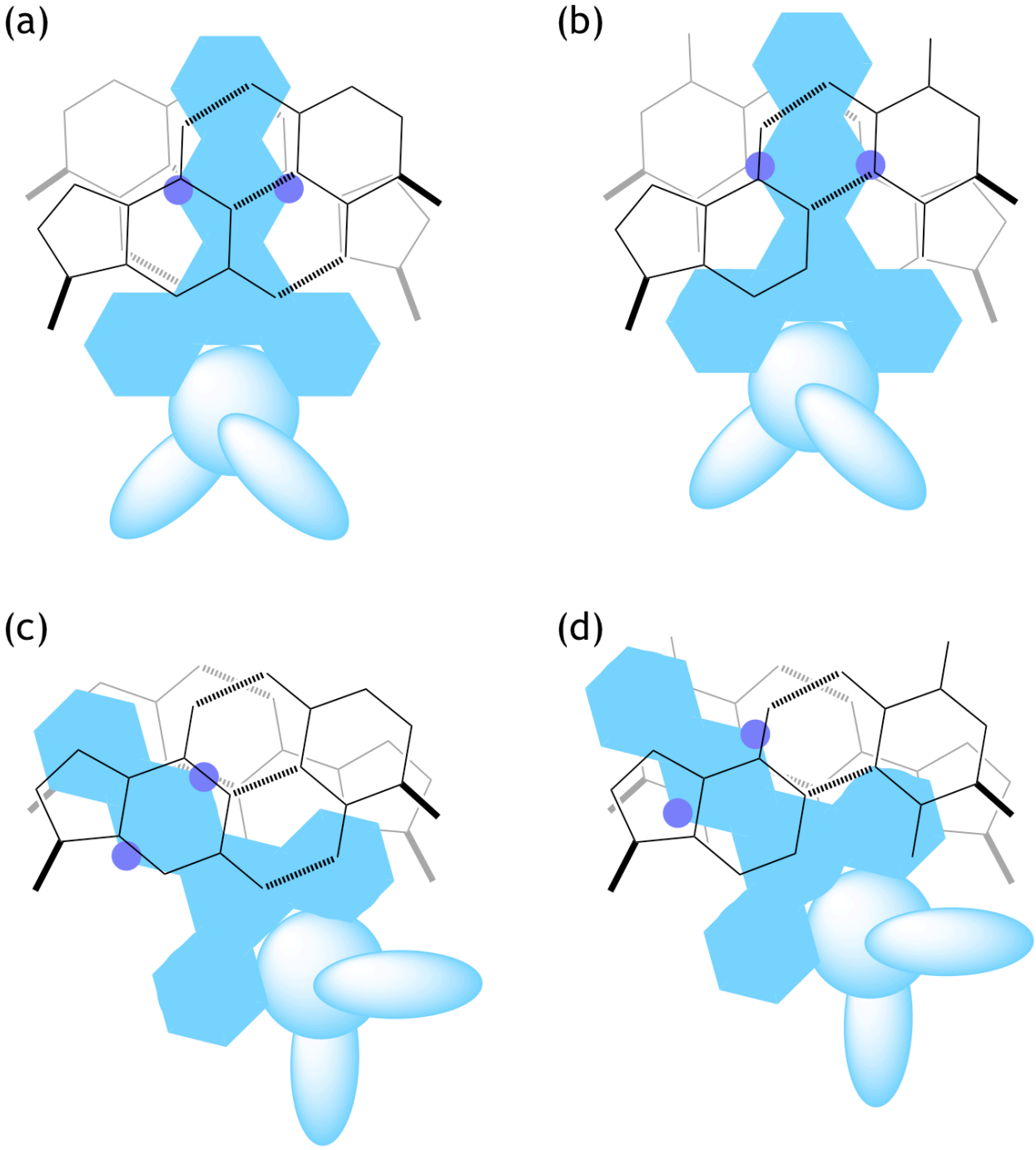

FIGURE 9. Cartoons to compare symmetic (a/b) and canted (c/d) intercalation of Δ-$[Ru(L)_2dppz]^{2+}$ at (a/c) $[GC]_2$ and (b/d) $[AT]_2$ steps.

	Δ-[Ru(phen)$_2$dppz]$^{2+}$				Λ-[Ru(phen)$_2$dppz]$^{2+}$			
[Nu]/[Ru]	τ_L / ns	α_L / %	τ_S / ns	α_S / %	τ_L / ns	α_L / %	τ_S / ns	α_S / %
2	464	*57*	68	*43*	243	*47*	53	*53*
4	700	*67*	143	*33*	298	*57*	54	*43*
6	673	*70*	116	*30*	323	*45*	40	*55*
8	791	*62*	144	*38*	331	*35*	42	*65*
12.5	756	*56*	129	*44*	352	*25*	44	*75*
25	739	*42*	132	*58*	325	*18*	38	*82*
50	737	*26*	135	*74*	327	*10*	36	*90*
100	727	*18*	137	*82*	329	*9*	36	*91*
τ_{av} (SD)	732 (38)		134 (10)		327 (15)		42 (6)	

TABLE S1. Time-resolved emission of [Ru(phen)$_2$dppz]$^{2+}$ enantiomers with [poly(dA-dT)]$_2$.
[Ru] = 20 μM; 5 mM phosphate (pH 6.9); 25 ^{o}C; λ_{ex} = 440 nm; λ_{em} >540 nm. τ_i = emission lifetime; α_i = pre-exponential factor.

	Δ-[Ru(phen)$_2$dppz]$^{2+}$				Λ-[Ru(phen)$_2$dppz]$^{2+}$			
[Nu]/[Ru]	τ_L / ns	α_L / %	τ_S / ns	α_S / %	τ_L / ns	α_L / %	τ_S / ns	α_S / %
2	174	*35*	54	*65*	116	*29*	37	*71*
4	241	*39*	71	*61*	108	*45*	41	*55*
6	257	*57*	69	*43*	108	*31*	47	*69*
8	260	*67*	64	*33*	136	*13*	48	*87*
12.5	254	*73*	61	*27*	139	*9*	42	*91*
25	256	*77*	76	*23*	164	*5*	40	*95*
50	248	*78*	67	*22*	165	*4*	41	*96*
100	255	*80*	90	*20*	168	*3*	39	*97*
τ_{av} (SD)	253 (6)		71 (10)		138 (26)		42 (4)	

TABLE S2. Time-resolved emission of [Ru(phen)$_2$dppz]$^{2+}$ enantiomers with [poly(dG-dC)]$_2$.
[Ru] = 20 μM; 5 mM phosphate (pH 6.9); 25 ^{o}C; λ_{ex} = 440 nm; λ_{em} >540 nm. τ_i = emission lifetime; α_i = pre-exponential factor.

	Δ-$[Ru(bpy)_2dppz]^{2+}$				Λ-$[Ru(bpy)_2dppz]^{2+}$			
[Nu]/[Ru]	τ_L / ns	α_L / %	τ_S / ns	α_S / %	τ_L / ns	α_L / %	τ_S / ns	α_S / %
2	363	*30*	122	*70*	254	*52*	41	*48*
4	410	*24*	136	*76*	285	*48*	47	*52*
6	460	*10*	128	*90*	311	*37*	46	*63*
8	473	*7*	118	*93*	295	*33*	39	*67*
12.5	561	*3*	117	*97*	296	*27*	42	*73*
25	-	-	106	*100*	233	*23*	31	*77*
50	-	-	114	*100*	249	*13*	32	*87*
100	-	-	107	*100*	210	*12*	29	*88*
τ_{av} (SD)	476 (63)		115 (10)		267 (35)		38 (7)	

TABLE S3. Time-resolved emission of $[Ru(bpy)_2dppz]^{2+}$ enantiomers with $[poly(dA\text{-}dT)]_2$.
[Ru] = 20 μM; 5 mM phosphate (pH 6.9); 25 °C; λ_{ex} = 440 nm; λ_{em} >540 nm. τ_i = emission lifetime; α_i = pre-exponential factor.

	Δ-$[Ru(bpy)_2dppz]^{2+}$				Λ-$[Ru(bpy)_2dppz]^{2+}$			
[Nu]/[Ru]	τ_L / ns	α_L / %	τ_S / ns	α_S / %	τ_L / ns	α_L / %	τ_S / ns	α_S / %
2	249	*18*	80	*82*	71	*55*	23	*45*
4	196	*44*	56	*56*	74	*63*	24	*37*
6	223	*55*	64	*45*	77	*59*	35	*41*
8	223	*63*	71	*37*	70	*68*	31	*32*
12.5	223	*66*	88	*34*	68	*63*	36	*37*
25	205	*82*	50	*18*	65	*72*	32	*28*
50	201	*83*	52	*17*	60	*81*	22	*19*
100	192	*83*	50	*17*	56	*94*	35	*6*
τ_{av} (SD)	209 (14)		62 (14)		63 (9)		32 (5)	

TABLE S4. Time-resolved emission of $[Ru(bpy)_2dppz]^{2+}$ enantiomers with $[poly(dG\text{-}dC)]_2$.
[Ru] = 20 μM; 5 mM phosphate (pH 6.9); 25 °C; λ_{ex} = 440 nm; λ_{em} >540 nm. τ_i = emission lifetime; α_i = pre-exponential factor.

	L = phen				L = bpy			
	τ_L/ns	α_L/%	τ_S/ns	α_S/%	τ_L/ns	α_L/%	τ_S/ns	α_S/%
C4 dimer	-	-	-	-	328	*23*	111	*77*
monomer[a]	737	*26*	135	*74*	-	-	114	*100*
CPI[b]	678	*10*	139	*90*	-	-	-	-
C2 dimer	468	*28*	153	*72*	206	*36*	94	*64*

TABLE S5. Time-resolved emission of Δ-$[Ru(L)_2dppz]^{2+}$ monomers and Δ,Δ-$[m\text{-}cx(cdppz)_2(L)_4Ru_2]^{4+}$ dimers (x = 2 or 4) with $[poly(dA\text{-}dT)]_2$ at [Nu]/[Ru] = 50.
[Ru] = 20 μM; 5 mM phosphate (pH 6.9); 25 °C; λ_{ex} = 440 nm; λ_{em} >540 nm. τ_i = emission lifetime; α_i = pre-exponential factor. [a] For the monomeric complexes, the quoted lifetimes and pre-exponential factors are the values shown in Tables S1-S4. [b] [Nu]/[Ru] = 70.

	L = phen				L = bpy			
	τ_L/ns	α_L/%	τ_S/ns	α_S/%	τ_L/ns	α_L/%	τ_S/ns	α_S/%
C4 dimer	789	*59*	158	*41*	363	*21*	118	*79*
monomer[a]	732	*59*	134	*41*	476	*5*	115	*95*
CPI[b]	635	*32*	122	*68*	-	-	-	-
C2 dimer	489	*28*	153	*72*	194	*46*	86	*54*

TABLE S6. Time-resolved emission of Δ-$[Ru(L)_2dppz]^{2+}$ monomers and Δ,Δ-$[m\text{-}cx(cdppz)_2(L)_4Ru_2]^{4+}$ dimers (x = 2 or 4) with $[poly(dA\text{-}dT)]_2$ at [Nu]/[Ru] = 10.
[Ru] = 20 μM; 5 mM phosphate (pH 6.9); 25 °C; λ_{ex} = 440 nm; λ_{em} >540 nm. τ_i = emission lifetime; α_i = pre-exponential factor. [a] For the monomeric complexes, the quoted lifetimes are the average values shown in Tables S1-S4; pre-exponential factors are the mean of the values obtained at [Nu]/[Ru] = 8 and 12.5. [b] [Nu]/[Ru] = 18.

	L = phen				L = bpy			
	τ_L/ns	α_L/%	τ_S/ns	α_S/%	τ_L/ns	α_L/%	τ_S/ns	α_S/%
C4 dimer[b]	-	-	-	-	373	*26*	118	*74*
C4 dimer[c]	-	-	-	-	340	*32*	122	*68*
monomer[a]	700	*67*	143	*33*	410	*24*	136	*76*
CPI	664	*74*	128	*26*	-	-	-	-
C2 dimer[b]	-	-	-	-	185	*49*	89	*51*
C2 dimer[c]	554	*22*	160	*78*	226	*24*	111	*76*

TABLE S7. Time-resolved emission of Δ-$[Ru(L)_2dppz]^{2+}$ monomers and Δ,Δ-$[m\text{-}cx(cdppz)_2(L)_4Ru_2]^{4+}$ dimers (x = 2 or 4) with $[poly(dA\text{-}dT)]_2$ at [Nu]/[Ru] = 4.
[Ru] = 20 μM; 5 mM phosphate (pH 6.9); 25 °C; λ_{ex} = 440 nm; λ_{em} >540 nm. τ_i = emission lifetime; α_i = pre-exponential factor. [a] For the monomeric complexes, the quoted lifetimes and pre-exponential factors are the values shown in Tables S1-S4. [b] values measured immediately after mixing. [c] values measured after 5 hours equilibration at 50 °C.

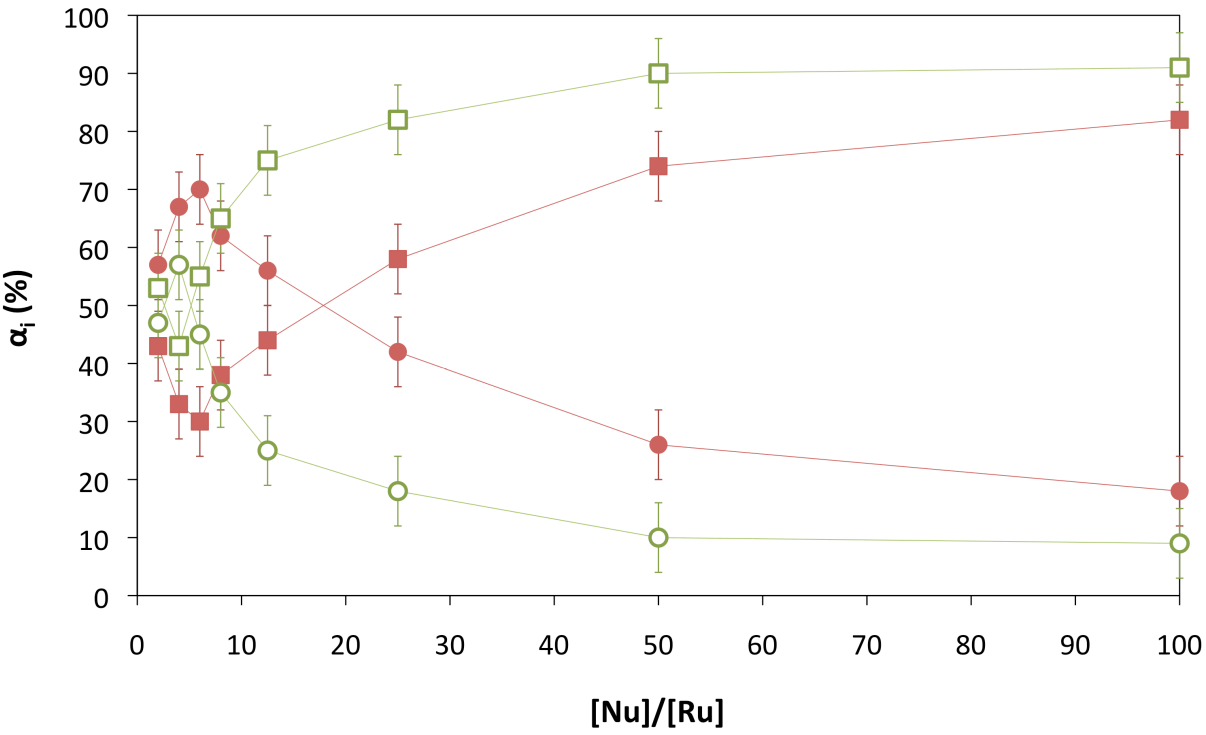

FIGURE S1. Pre-exponential factors (α_i) for enantiomers of $[Ru(phen)_2dppz]^{2+}$ bound to $[poly(dA\text{-}dT)]_2$ in 5 mM phosphate (pH 6.9) buffer. Δ- = closed symbols; τ_L = 732 (38) ns, ●; τ_S = 134 (10) ns, ■. Λ- = open symbols; τ_L = 327 (15) ns, ○; τ_S = 42 (6) ns, □. [Ru] = 20 μM. λ_{ex} = 440 nm; λ_{em} > 540 nm.

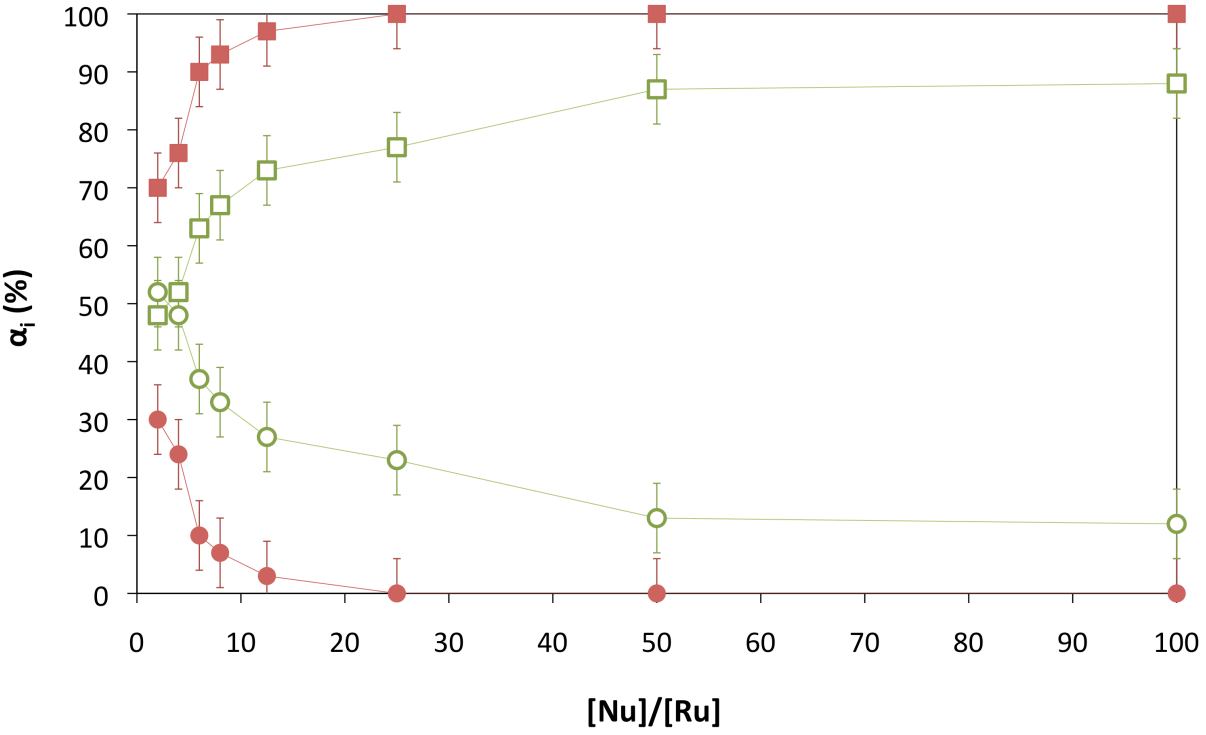

FIGURE S2. Pre-exponential factors (α_i) for enantiomers of $[Ru(bpy)_2dppz]^{2+}$ bound to $[poly(dA\text{-}dT)]_2$ in 5 mM phosphate (pH 6.9) buffer. Δ- = closed symbols; τ_L = 476 (63) ns, ●; τ_S = 115 (10) ns, ■. Λ- = open symbols; τ_L = 267 (35) ns, ○; τ_S = 38 (7) ns, □. [Ru] = 20 μM. λ_{ex} = 440 nm; λ_{em} > 540 nm.

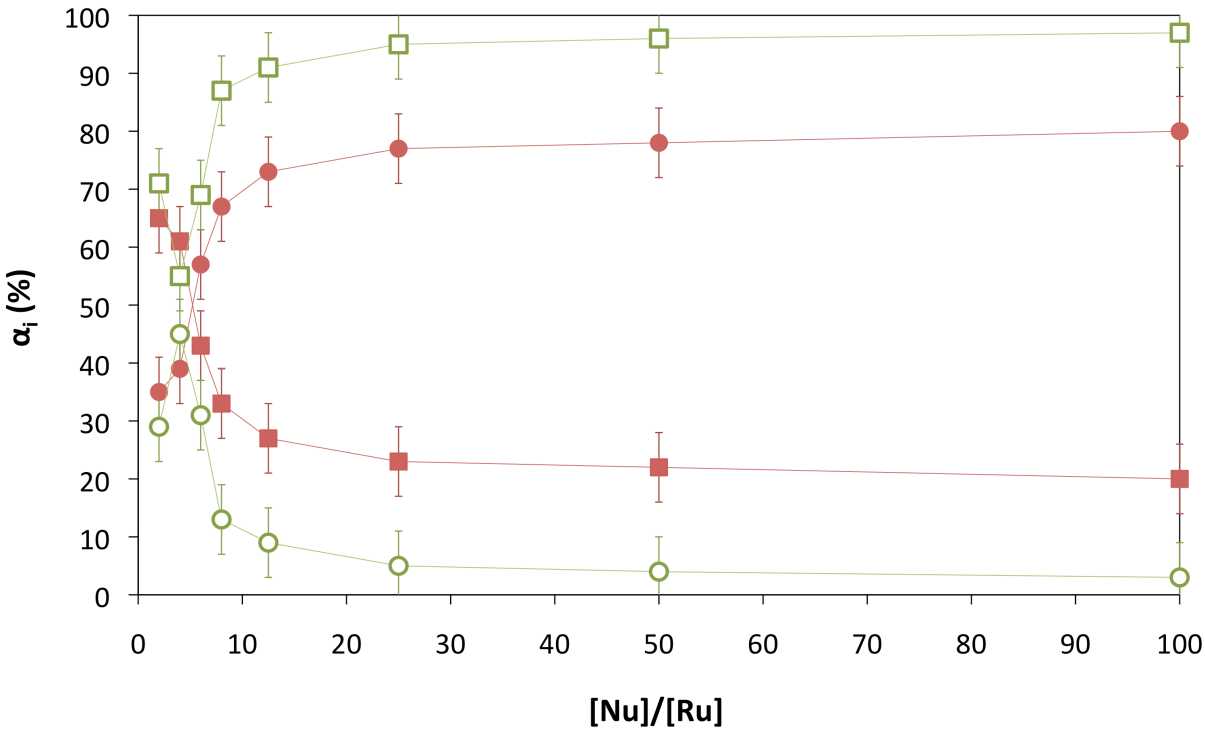

FIGURE S3. Pre-exponential factors (α_i) for enantiomers of $[Ru(phen)_2dppz]^{2+}$ bound to $[poly(dG\text{-}dC)]_2$ in 5 mM phosphate (pH 6.9) buffer. Δ- = closed symbols; τ_L = 253 (6) ns, ●; τ_S = 71 (10) ns, ■. Λ- = open symbols; τ_L = 138 (26) ns, ○; τ_S = 42 (4) ns, □. [Ru] = 20 μM. λ_{ex} = 440 nm; λ_{em} > 540 nm.

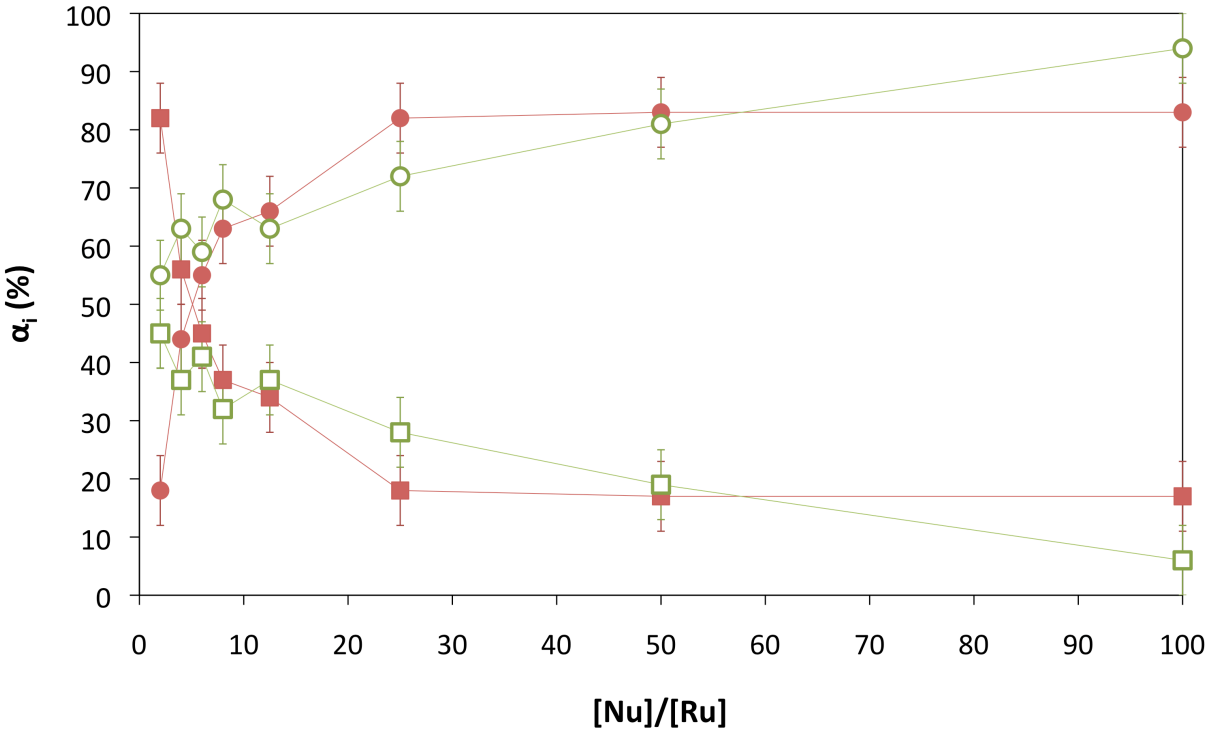

FIGURE S4. Pre-exponential factors (α_i) for enantiomers of $[Ru(bpy)_2dppz]^{2+}$ bound to $[poly(dG\text{-}dC)]_2$ in 5 mM phosphate (pH 6.9) buffer. Δ- = closed symbols; τ_L = 209 (14) ns, ●; τ_S = 62 (14) ns, ■. Λ- = open symbols; τ_L = 63 (9) ns, ○; τ_S = 32 (5) ns, □. [Ru] = 20 μM. λ_{ex} = 440 nm; λ_{em} > 540 nm.

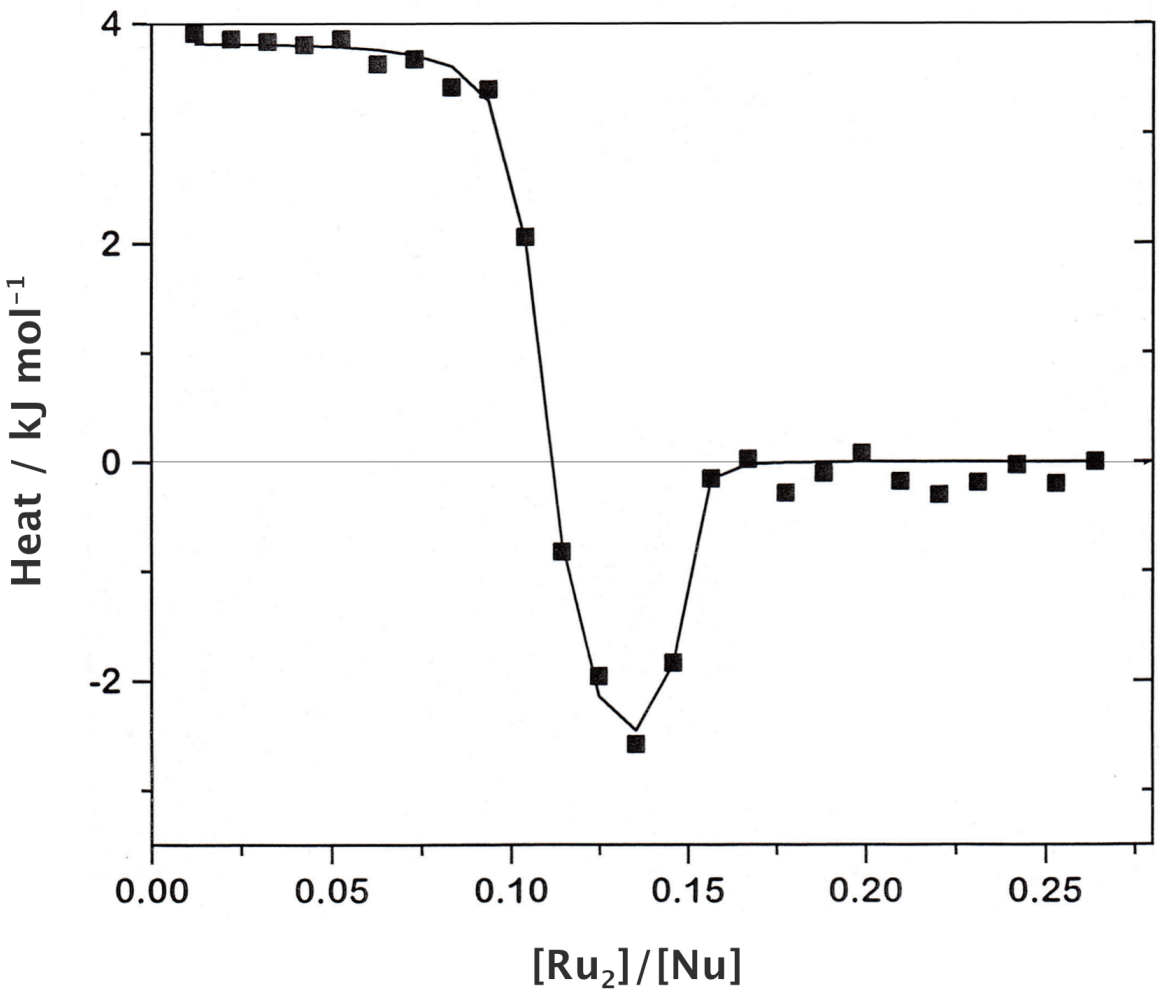

FIGURE S5. Isothermal Titration Calorimetry for Δ,Δ-[μ-c4(cdppz)$_2$(phen)$_4$Ru$_2$]$^{4+}$ added to CT-DNA. [DNA] = 100 μM; 5 mM phosphate buffer (pH 6.9); 20 ^{o}C.

Calculation of Diffusion-Controlled Rate Constant

(i) Derivation of Equations

For a reaction occurring between two species of similar size, the diffusion-controlled rate constant, k_d may be determined from Equation A.1.

$$k_d = \frac{8RT}{3\eta} \tag{A.1}$$

where R is the Gas constant (8.3145 J K^{-1} mol^{-1}), η is solvent viscosity, and T is absolute temperature. However, for this work, it was necessary to take into account the difference in size of the reacting species, in this case the size of the $[Ru(phen)_2dppz]^{2+}$ and 2-deoxyguanosine in DMF.

The combination of Fick's First law and the diffusion equation gives Equation A.2

$$k_d = 4\pi R^* D N_A \tag{A.2}$$

where D is the sum of the diffusion coefficients of the two species ($D = D_A + D_B$.), R^* is the distance at which the reaction occurs, approximated as $R^* = R_A + R_B$, where R_i is the molecular radius of species i, and N_A is Avogadro's number (6.02214×10^{23} mol^{-1}).

Incorporating the Stokes-Einstein equation (A.3) for diffusion coefficients of spherical molecules,

$$D_A = \frac{k_B T}{6\pi\eta R_A} \qquad D_B = \frac{k_B T}{6\pi\eta R_B} \tag{A.3}$$

where k_B is Boltzmann's constant (1.38065×10^{-23} m^2 kg s^{-2} K^{-1}), we obtain the sum diffusion coefficient as Equation A.4.

$$D = \frac{k_B T}{6\pi\eta}\left(\frac{1}{R_A} + \frac{1}{R_B}\right) = \frac{k_B T}{6\pi\eta}\left(\frac{R_A + R_B}{R_A R_B}\right) \tag{A.4}$$

From this, the rate constant is calculated according to Equation A.5.

$$k_d = 4\pi\left(R_A + R_B\right)\frac{k_B T}{6\pi\eta}\left(\frac{R_A + R_B}{R_A R_B}\right)N_A = \frac{2RT}{3\eta}\frac{\left(R_A + R_B\right)^2}{R_A R_B} \tag{A.5}$$

For $R_A = R_B$, this reduces to Equation A.1.

(ii) Estimating Molecular Radii

One problem with this formulation is that it requires an estimation of the molecular radius of each of the molecules involved in the quenching process. For simple molecules, *e.g.* molecular oxygen, the radius is fairly simple to estimate, however for the larger ruthenium complexes, the estimation is more complex. Approximating the quasi-propeller-shaped ruthenium complexes as a sphere is less than ideal, however for the purposes of this quenching model an `average' radius needs to be determined. Modelling calculations were performed using the Spartan molecular modelling application.

The general method used to estimate the radius of the molecule is as follows:

a. The molecule was drawn in Spartan.
b. If the molecule did not already exist in the software database, the structure of the model was optimised with the `minimise structure' command.
c. The surface area and volume of the CPK space-filling molecule were determined.
d. The volume and surface areas were used to calculate a 'radius' for the molecule, assuming a sphere.

There is a substantial variation in the radius resulting from each of these parameters (CPK volume, surface area and diameter). The diameter parameter simply states the distance between the two atoms with the greatest separation. Understandably this will not provide an accurate value for small molecules (*e.g.* molecular oxygen), however for larger molecules the value becomes more useful. In light of this, it was

decided to use the surface area parameter to define the spherical radius approximation for each molecule as it takes into account the fact that the molecules under consideration are not spherical and have a large surface presented to the encapsulating solvent.

Calculated Radii for $[Ru(phen)_2dppz]^{2+}$

CPK volume	656.78 $Å^3$	R = 5.392 Å
CPK surface area	660.82 $Å^2$	R = 7.252 Å
Diameter	15.2 Å	R = 7.60 Å

Calculated Radii for 2'-deoxyguanosine

CPK volume	286.60 $Å^3$	R = 4.090 Å
CPK surface area	324.42 $Å^2$	R = 5.081 Å
Diameter	13.55 Å	R = 6.775 Å

(iii) Calculation of Diffusion-Controlled Rate Constant

For experiments in DMF, the diffusion controlled rate constant assuming equal molecular dimensions is 7.03×10^9 mol^{-1} dm^3 s^{-1} at 293.15 K, with a DMF viscosity of η = 0.924 mPa s [J. Riddick, W. Bunger, & T. Sakano, editors, Organic Solvents, Wiley-Interscience, New York, 4th edition, 1986.]

DMF viscosity data [J. Riddick, W. Bunger, and T. Sakano, editors, Organic Solvents, Wiley-Interscience, New York, 4th edition, 1986.]

20 ^oC η = 0.924 mPa s = 9.24×10^{-4} kg m^{-1} s^{-1}
25 ^oC η = 0.802 mPa s = 8.02×10^{-4} kg m^{-1} s^{-1}
40 ^oC η = 0.739 mPa s = 7.39×10^{-4} kg m^{-1} s^{-1}

Using the equation for unequal radii, we obtain the following diffusion coefficients for $[Ru(phen)_2dppz]^{2+}$ and 2'-deoxyguanosine in DMF at 293.15 K:
$[Ru(phen)_2dppz]^{2+}$ R = 7.252 Å; $D = 3.20 \times 10^{-10}$ m^2 s^{-1}
2'-deoxyguanosine R = 5.081 Å; $D = 4.57 \times 10^{-10}$ m^2 s^{-1}

This gives the diffusion-controlled rate constant for reaction between $[Ru(phen)_2dppz]^{2+}$ and 2'-deoxyguanosine in DMF at 293.15 K as:
$k_d = 7.3 \times 10^9$ dm^3 s^{-1} mol^{-1}

Calculation of Driving Force for Photoinduced Electron Transfer

The proposed mechanism of quenching involves reduction of the excited emissive ^{3}MLCT state of $[Ru^{II}(phen)_2dppz]^{2+}$ by 2'-dG.
Reduction of the ^{3}MLCT state of the metal complex by nucleosides can be described thus:

$$[Ru^{II}(phen)_2dppz]^{2+} + dN \Leftrightarrow *[Ru^{III}(phen)_2(dppz^{\cdot-})]^{2+} + dN \Leftrightarrow [Ru^{II}(phen)_2(dppz^{\cdot-})]^{+} + dN^{\cdot+}$$

In general, the driving force for photoinduced oxidation of nucleobases, ΔG^o_{ox}, is given by the Rehm-Weller Equation (B.1), where $E^o(D^{\cdot+}/D)$ is the standard potential for oxidation of the electron donor, $E^o(A/A^{\cdot-})$ is the standard potential for reduction of the electron acceptor, and $E_{0,0}(C)$ is the energy of the excited state. For the reaction above, it is the acceptor, $[Ru(phen)_2dppz]^{2+}$, which is excited; hence $E_{0,0}(C)$ is obtained from the ^{3}MLCT emission.

$$\Delta G^o_{ET} = E^o(N^{\bullet+}/N) - E^o(A/A^{\bullet-}) - E_{0,0}(A) + \Delta G^o_{\varepsilon} \qquad \text{(B.1)}$$

ΔG^o_{ε} is a coulombic term based on the Born Equation that is applied to correct for the dielectric character of the solvent, calculated from Equation B.2.

$$\Delta G^o(\varepsilon) = \frac{e^2}{4\pi\varepsilon_0}\left[\left(\frac{1}{r_{ion}} - \frac{1}{a_{EC}}\right)\frac{1}{\varepsilon_s} - \frac{1}{r_{ion}\varepsilon_{org}}\right] \qquad \text{(B.2)}$$

In this equation, e is the fundamental charge (1.602×10^{-19} C), ε_0 is the permittivity of vacuum (8.854×10^{-12} F m^{-1}), r_{ion} is the radius of the radical ion, a_{EC} is the center-to-center separation between the donor and acceptor in the encounter complex, ε_s is the dielectric constant of the solvent in which the reaction occurs, while ε_{org} is the dielectric constant of the solvent in which the redox properties are measured. Typically, for a quenching reaction in water relative to potentials measured in organic solvents are $\Delta G^o(\varepsilon) \approx$ -0.1 eV. For the solvent change MeCN/DMF, the value is ≈ -0.03 eV.

For the ground state reduction of $[Ru(phen)_2dppz]^{2+}$,

$$[Ru^{II}(phen)_2dppz]^{2+} + e^- \Leftrightarrow [Ru^{I}(phen)_2dppz]^{+}$$

Ortmans and coworkers [I. Ortmans, B. Elias, J. M. Kelly, C. Moucheron, & A. Kirsch-De Mesmaeker, *Dalton Trans.* 2004 , 668] reported the potential to be -1.00 V *vs* SCE (-0.76 V *vs* NHE). In DMF, the emission maximum is observed at 634 nm (1.96 eV).

Seidel and coworkers [C. A. M. Seidel, A. Schulz, & M. H. M. Sauer, *J. Phys. Chem.* **1996**, *100*, 5541-5543.] measured the redox properties of the four primary nucleobases in aprotic solvents, along with the necessary correction factors to adjust these values to aqueous solvents. They reported the oxidation potentials in acetonitrile and reduction potentials in dimethyl formamide.

For oxidation of deoxynucleosides,

$$dN^{\cdot+} + e^- \Leftrightarrow dN$$

the experimental oxidation potentials determined by cyclic voltammetry in acetonitrile are reported below, and the values in DMF are ≈ 0.03 V lower.

Standard potentials for oxidation of nucleosides [$E^o(N^{\cdot+}/N)$, V vs NHE, ±0.05 V] in CH_3CN [C. A. M. Seidel, A. Schulz, & M. H. M. Sauer, J. Phys. Chem. 1996, 100, 5541-5543.].

Nucleoside	E^o_{MeCN}
Guanosine	1.47 V
Adenosine	1.94 V
Cytidine	2.12 V
Thymidine	2.09 V

Driving forces for quenching of ruthenium luminescence by oxidation of mononucleosides

Mononucleoside	ΔG^o_{ox}
2'-dG	+0.24 V
2'-dA	+0.71 V
2'-dT	+0.89 V
2'-dC	+0.86 V

From this calculation, oxidation by any nucleoside is unfavourable. However, since all potentials are not measured in the same solvent under the same conditions, the figures may not represent accurateyl, the absolute values. Nevertheless, the trend in driving force is likely correct. Quenching by oxidation of 2'-dG is the least disfavoured process by 0.5 V. Thus, if this reaction occurs with an activation-controlled rate constant, then quenching by the other nucleosides is not likely to be favourable.
The driving force for quenching by reduction of any nucleoside is very unfavourable (>1.7 eV), and cannot be a competing reaction.